Article

Cell Reports

Synthetic Essentiality of Metabolic Regulator PDHK1 in PTEN-Deficient Cells and Cancers

Graphical Abstract

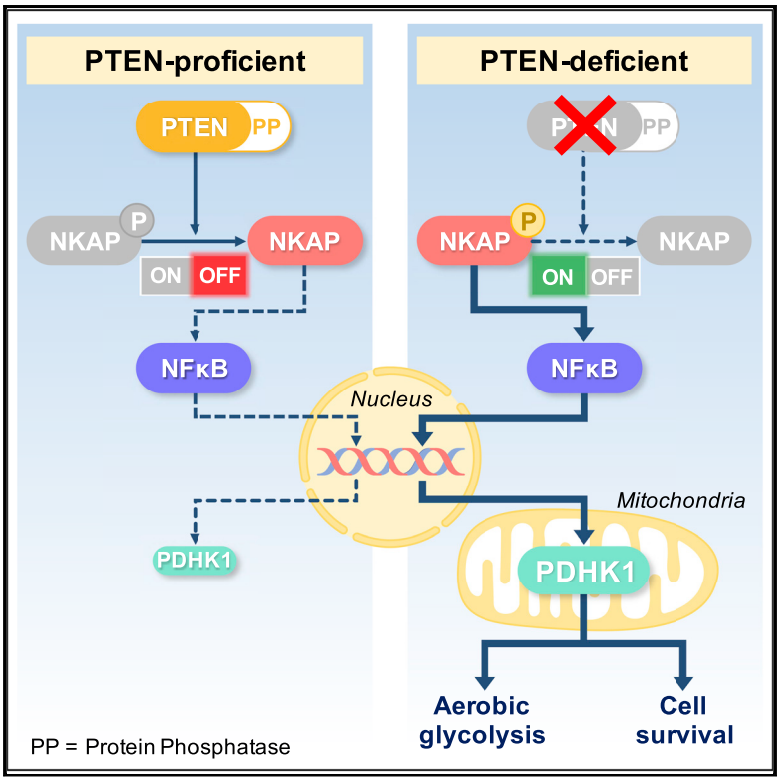

Authors

Nilanjana Chatterjee, Evangelos Pazarentzos, Manasi K. Mayekar, ..., Asmin Tulpule, Amit J. Sabnis, Trever G. Bivona

Correspondence

nilanjana.chatterjee@ucsf.edu (N.C.), trever.bivona@ucsf.edu (T.G.B.)

In Brief

The tumor suppressor PTEN is widely inactivated in cancers and tumor syndromes. Currently, there is no effective therapeutic strategy in the clinic for PTEN-deficient cancers. Chatterjee et al. found that PTEN-deficient cells and cancers are uniquely sensitive to PDHK1 inhibition and propose PDHK1 as a potential therapeutic target in PTEN-deficient cancers.

Highlights

- PDHK1 is a synthetic-essential gene in PTEN-deficient normal and cancer cells
- PTEN-PP dephosphorylates NKAP to suppress NF-κB activation and PDHK1 expression
- PTEN-PP loss upregulates PDHK1 and promotes glycolysis and PDHK1 cellular dependence
- High PDHK1 levels in PTEN-deficient tumors correlate with inferior patient survival

Chatterjee et al., 2019, Cell Reports *28*, 2317–2330
August 27, 2019
https://doi.org/10.1016/j.celrep.2019.07.063

CellPress

Cell Reports
Article

Synthetic Essentiality of Metabolic Regulator PDHK1 in PTEN-Deficient Cells and Cancers

Nilanjana Chatterjee,[1,2,10,*] Evangelos Pazarentzos,[1,2,10] Manasi K. Mayekar,[1,2] Philippe Gui,[1,2] David V. Allegakoen,[1,2] Gorjan Hrustanovic,[1,2] Victor Olivas,[1,2] Luping Lin,[1,2] Erik Verschueren,[3,4,5] Jeffrey R. Johnson,[3,4,5] Matan Hofree,[6] Jenny J. Yan,[1,2] Billy W. Newton,[3,4,5] John V. Dollen,[3,4,5] Charles H. Earnshaw,[1] Jennifer Flanagan,[1,2] Elton Chan,[1,2] Saurabh Asthana,[2] Trey Ideker,[6] Wei Wu,[1,2] Junji Suzuki,[8] Benjamin A. Barad,[7] Yuriy Kirichok,[8] James S. Fraser,[7] William A. Weiss,[9] Nevan J. Krogan,[3,4,5] Asmin Tulpule,[2] Amit J. Sabnis,[2] and Trever G. Bivona[1,2,4,5,11,*]
[1]Department of Medicine, University of California, San Francisco, San Francisco, CA 94158, USA
[2]Helen Diller Family Comprehensive Cancer Center, University of California, San Francisco, San Francisco, CA 94158, USA
[3]J. David Gladstone Institutes, San Francisco, CA 94158, USA
[4]Department of Cellular and Molecular Pharmacology, University of California, San Francisco, San Francisco, CA 94158, USA
[5]QB3, California Institute for Quantitative Biosciences, San Francisco, CA 94158, USA
[6]Department of Bioengineering, University of California, San Diego, San Diego, CA 92093, USA
[7]Department of Bioengineering and Therapeutic Sciences, University of California, San Francisco, San Francisco, CA 94158, USA
[8]Department of Physiology, University of California, San Francisco, San Francisco, CA 94158, USA
[9]Department of Neurology, University of California, San Francisco, San Francisco, CA 94143, USA
[10]These authors contributed equally
[11]Lead Contact
*Correspondence: nilanjana.chatterjee@ucsf.edu (N.C.), trever.bivona@ucsf.edu (T.G.B.)
https://doi.org/10.1016/j.celrep.2019.07.063

SUMMARY

Phosphatase and tensin homolog deleted on chromosome 10 (PTEN) is a tumor suppressor and bifunctional lipid and protein phosphatase. We report that the metabolic regulator pyruvate dehydrogenase kinase1 (PDHK1) is a synthetic-essential gene in PTEN-deficient cancer and normal cells. The PTEN protein phosphatase dephosphorylates nuclear factor κB (NF-κB)-activating protein (NKAP) and limits NFκB activation to suppress expression of PDHK1, a NF-κB target gene. Loss of the PTEN protein phosphatase upregulates PDHK1 to induce aerobic glycolysis and PDHK1 cellular dependence. PTEN-deficient human tumors harbor increased PDHK1, a biomarker of decreased patient survival. This study uncovers a PTEN-regulated signaling pathway and reveals PDHK1 as a potential target in PTEN-deficient cancers.

INTRODUCTION

Phosphatase and tensin homolog deleted on chromosome 10 (PTEN) is a tumor suppressor with both lipid and protein phosphatase activities (Li and Sun, 1997; Li et al., 1997; Maehama and Dixon, 1998, 1999, 2000; Myers et al., 1997, 1998; Steck et al., 1997). As a lipid phosphatase, PTEN antagonizes PI3K/AKT/mTOR signaling through de-phosphorylation of the lipid second messenger PIP3 (phosphatidylinositol-3,4,5 triphosphate) to PIP2 (phosphatidylinositol-4,5 bisphosphate), regulating cellular metabolism, growth, and survival (Chalhoub and Baker, 2009; Lee et al., 1999; Maehama and Dixon, 1998; Myers et al., 1998; Stambolic et al., 1998).

PTEN can also function through protein phosphatase-dependent mechanisms (Davidson et al., 2010; Gildea et al., 2004; Leslie et al., 2009; Myers et al., 1997). A growing body of literature supports biological roles for the PTEN protein phosphatase (Dey et al., 2008; Gu et al., 2011; Hlobilkova et al., 2000; Leslie et al., 2007; Shi et al., 2014; Shinde and Maddika, 2016; Tibarewal et al., 2012; Wozniak et al., 2017; You et al., 2015). The modest clinical activity of PI3K and AKT inhibitors in PTEN-deficient cancers (Chandarlapaty et al., 2011; Ghosh et al., 2013; Rodon et al., 2013) coupled with the existence of tumor-derived PTEN Y138 mutants, which specifically lack the protein phosphatase activity (Davidson et al., 2010; Tibarewal et al., 2012), suggest that protein phosphatase-dependent cellular processes may contribute to PTEN-mediated tumor suppression. We investigated activity-specific PTEN functions to identify vulnerabilities for therapeutic exploitation to improve the treatment of PTEN-deficient cancers.

RESULTS

PTEN Deficiency Upregulates PDHK1 Expression in Normal and Cancer Cells

To uncover molecular events through which PTEN functions, we investigated gene expression changes in PTEN-deficient human lung adenocarcinoma H1650 cells (Table S1) in comparison with the matched cell line into which wild-type (WT) PTEN was re-introduced. Stable PTEN re-expression suppressed phospho-AKT levels (Figure 1A), as expected (Sos et al., 2009). By unbiased comparative gene expression profiling analysis, we identified 52 significantly differentially regulated genes (fold change > 2, $p < 0.05$, $q < 0.2$) between the PTEN re-expressing H1650 and

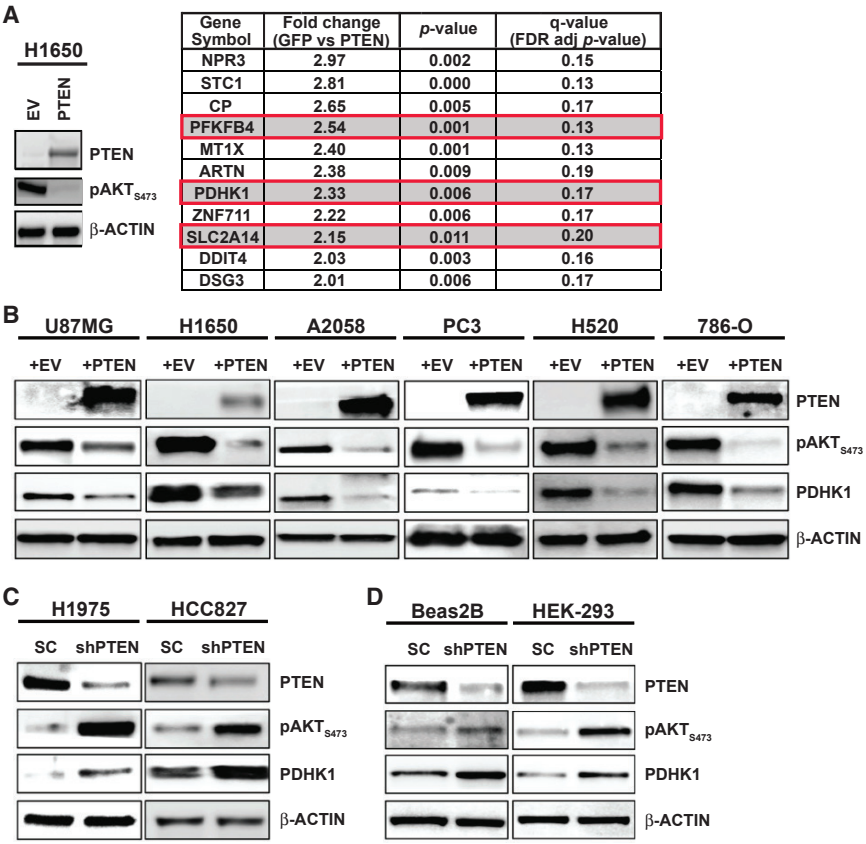

Gene Symbol	Fold change (GFP vs PTEN)	*p*-value	q-value (FDR adj *p*-value)
NPR3	2.97	0.002	0.15
STC1	2.81	0.000	0.13
CP	2.65	0.005	0.17
PFKFB4	2.54	0.001	0.13
MT1X	2.40	0.001	0.13
ARTN	2.38	0.009	0.19
PDHK1	2.33	0.006	0.17
ZNF711	2.22	0.006	0.17
SLC2A14	2.15	0.011	0.20
DDIT4	2.03	0.003	0.16
DSG3	2.01	0.006	0.17

Figure 1. PTEN Loss or Inactivation Upregulates PDHK1 in Cancer and Normal Cells

(A) Left: western blots showing PTEN and phospho-AKT expression in PTEN-deficient H1650 cancer cells stably expressing PTEN or empty vector (EV). Right: list of genes significantly upregulated (fold change > 2, multiple t tests, *$p < 0.05$, $q < 0.2$, $n = 3$ replicates) in GFP-expressing H1650 cells compared with H1650 cells stably re-expressing PTEN, by microarray analysis. Highlighted in red boxes are the top upregulated energy metabolism genes, including PDHK1, in H1650-GFP cells.

(B) Western blots showing PTEN, phospho-AKT, and PDHK1 expression in PTEN-deficient cancer cell lines stably expressing PTEN or empty vector (EV).

(C and D) Same as (B) in PTEN-proficient cancer (C) or normal (non-cancer) (D) cell lines with stable PTEN knockdown. shPTEN, shRNA to PTEN; SC, scrambled control shRNA.

See also Figure S1 and Tables S1 and S2.

PTEN-deficient H1650-GFP control cells (Figure 1A; Table S2). Re-introduction of PTEN in H1650 cells caused significant downregulation of 11 genes and upregulation of 41 genes. We found several energy metabolism genes including pyruvate dehydrogenase kinase 1 (PDHK1; gene name PDK1) among the genes that showed significant upregulation (>2-fold increase, $p < 0.05$, $q < 0.2$) in the PTEN-deficient H1650-GFP cells (Figure 1A, red boxes).

PDHK1 is a regulator of energy metabolism in cells (Schulze and Downward, 2011) with no known connection to PTEN, unlike the other top hit, 6-phosphofructo-2-kinase/fructose-2,6-bisphosphatase 4 (PFKFB4) (Figure 1A, red boxes), which regulates AKT, a known downstream effector of PTEN (Chesney et al., 2014; Figueiredo et al., 2017; Houddane et al., 2017; Sun et al., 1999). PDHK1 and other PDHK isoenzymes (PDHK2–4) phosphorylate the E1 alpha subunit (PDHA1) of the pyruvate dehydrogenase complex (PDC) that catalyzes oxidative decarboxylation of pyruvate to acetyl-CoA in mitochondria (Patel and Roche, 1990; Popov et al., 1997; Teague et al., 1979). Phosphorylation of PDHA1 inhibits PDC activity and blocks pyruvate entry into the tricarboxylic acid (TCA) cycle to uncouple glycolysis from the TCA cycle, contributing to the Warburg effect (Korotchkina and Patel, 2001; Linn et al., 1969; Vander Heiden et al., 2009; Warburg, 1956). Analysis of an independently conducted large-scale RNAi screening project (http://www.broadinstitute.org/achilles) showed that three of four PDHK1-targeted short hairpin RNAs (shRNAs) were depleted in H1650 cells, in which we observed PDHK1 upregulation (Figure 1A). These findings suggest that PDHK1 expression may be essential for PTEN-deficient H1650 cell growth. We hypothesized PDHK1 is an unrecognized PTEN effector through which PTEN regulates cellular energy metabolism and survival.

We assessed whether PDHK1 expression was regulated by PTEN across a panel of cancer and normal cell lines that either lack or stably express PTEN (Table S1) (Aguissa-Touré and Li, 2012; Koul, 2008; Lee et al., 2014; Pourmand et al., 2007; Sos et al., 2009). PDHK1 expression was decreased by PTEN re-expression in multiple PTEN-deficient models, such as lung adenocarcinoma (H1650), lung squamous cell carcinoma (H520), glioblastoma (U87MG), melanoma (A2058), prostate adenocarcinoma (PC3), and renal carcinoma cells (786-O) (Figures 1B and S1A; Table S1). PDHK1 expression was increased upon PTEN silencing in cancer cells and normal (non-cancer) cells that are otherwise PTEN proficient, such as lung adenocarcinoma (HCC827, H1975) and non-cancer cells (Beas2B, HEK293T) (Figures 1C, 1D, and S1A; Table S1). These findings indicate an inverse relationship in which PTEN status controls PDHK1 expression. Unlike PDHK1, other PDHK isoforms, including PDHK2, 3, and 4, exhibited lower expression in cancer cells, consistent with earlier studies (Grassian et al., 2011), and were not significantly modulated by PTEN levels (Figure S1B), suggesting specificity in the link between PTEN and PDHK1. Thus, PTEN loss specifically induces PDHK1 expression in cells.

Using an independently generated dataset (Pathak et al., 2013), we corroborated these findings *in vivo* and in non-malignant tissue. PDHK1 levels were higher in normal murine lung epithelium in which PTEN was genetically inactivated compared with $PTEN^{WT}$-expressing control mice (Figure S1C), suggesting physiological regulation of PDHK1 expression by PTEN *in vivo*.

We investigated whether PTEN-deficient human cancer specimens harbor increased PDHK1 levels. By immunohistochemistry

(IHC) analysis, we detected a significant inverse relationship between PDHK1 and PTEN expression levels in multiple human tumor types with frequent PTEN inactivation, including glioblastoma, prostate adenocarcinoma, and lung squamous cell carcinoma (Figures S2A–S2F). We found a strong association between PTEN inactivation and increased PDHK1 expression in a pan-cancer analysis across 12 different tumor types in The Cancer Genome Atlas (TCGA) dataset (Figure S2G). These data suggest clinical relevance of the PTEN/PDHK1 inverse relationship.

Analysis of the range of PDHK1 expression levels in these PTEN-deficient cancers showed that higher PDHK1 expression was a biomarker of decreased patient survival, suggesting that PDHK1 may contribute to PTEN's tumor suppressor function (Figure S2H). Our data reveal that PTEN loss promotes PDHK1 expression in malignant and normal cells and tissues and uncover increased PDHK1 levels in PTEN-deficient tumors as a biomarker of worse patient survival.

PTEN and PDHK1 Co-suppression Confers Synthetic Lethality in Normal and Cancer Cells

We investigated whether the PDHK1 upregulation induced by PTEN inactivation in cells is important for growth and survival. By silencing PDHK1 (using shRNAs to knockdown PDHK1) in PTEN-deficient and PTEN-proficient cells (Figures 2A, 2B, S3A, and S3B), we found that PDHK1 was essential for the survival of PTEN-deficient but not PTEN-expressing normal and cancer cells. The synthetic lethality conferred upon by PDHK1 co-suppression with PTEN loss in PTEN-deficient cells was rescued by re-expression of shRNA-resistant PDHK1 (Figure 2C).

We confirmed that treatment with the PDHK1 inhibitor DCA (dichloroacetate) (Kato et al., 2007; Stacpoole, 1989) suppressed phosphorylation of the PDHK1 target PDHA1, as expected (Whitehouse et al., 1974), in PTEN-deficient cells (Figure S3C). Although DCA may have off-target effects, the primary activity in the PTEN-deficient cells is likely via PDHK1 inhibition in these cells, as other known targets of DCA (e.g., PDHK2–4) were not expressed or not PTEN responsive in these systems (Figure S1B). PTEN status specifically dictated sensitivity to PDHK1 inhibition but not to cytotoxic chemotherapies (Figure S3D).

We next used the genetically controlled system of paired cell lines that stably lack or express PTEN. PDHK1 knockdown significantly decreased survival in normal and cancer cells specifically during PTEN co-suppression (Figure 2D). PDHK1 and PTEN co-suppression was lethal in cancer and normal cells, with evidence of enhanced apoptosis (Figures 2E and 2F). PDHK1 inhibition with DCA decreased phospho-PDHA1 levels, as expected (Whitehouse et al., 1974), and increased apoptosis specifically in PTEN-deficient cells with increased PDHK1 (Figure S3E). Thus, PDHK1 is essential for survival in PTEN-deficient cells.

We investigated the underlying mechanisms of the observed synthetic lethality and apoptosis induction by PTEN and PDHK1 co-suppression in normal and cancer cells. This lethality induced by PDHK1 suppression in PTEN-deficient cells is likely due to a loss of mitochondrial membrane potential (measured by mitochondrial matrix pH using an established ratiometric pH-sensitive probe SypHer-dmito; Perry et al., 2011; Poburko et al., 2011; Suzuki et al., 2014) upon PDHK1 inhibition, consistent with prior work (Bonnet et al., 2007) (Figure S4A). We found that A2058 PTEN-null melanoma cells exhibited higher mitochondrial matrix pH (higher SypHer-dmito ratio [F470/F430]), indicative of higher mitochondrial membrane potential, compared with A2058 cells with stable PTEN re-expression. These data are consistent with studies showing that PTEN-null mouse embryonic fibroblasts (MEFs) have higher mitochondrial membrane potential compared with MEFs with PTEN reconstitution (Goo et al., 2012). Upon acute inhibition of PDHK1 by DCA in PTEN-deficient cells, the mitochondrial membrane potential decreased (Figure S4A), consistent with data in other cancer cells (Bonnet et al., 2007). This decreased mitochondrial membrane potential upon PDHK1 suppression in PTEN-deficient cells likely underlies cell death (Figures 2 and S3). As a consequence of the mitochondrial membrane potential depolarization upon PDHK1 suppression in PTEN-deficient cells (Figure S4A), we found release of the apoptotic effector cytochrome *c* into the cytosol from the mitochondria (Figure S4B), activation of caspases 9, 7, and 3 (Figure S4C), and enhanced ROS (reactive oxygen species) generation (Figure S4D) that induce apoptosis (Figures 2 and S3). We also found that the decreased cell viability upon PDHK1 inhibition in PTEN-deficient cells was rescued by the stable overexpression of anti-apoptotic factors Bcl-xL or Bcl2 (Figures S4E and S4F), which can prevent cell death by limiting loss of mitochondrial membrane potential, release of cytochrome *c* into the cytoplasm, and caspase activation (Chinnaiyan et al., 1996; Shimizu et al., 1996a, 1996b, 1998; Tsujimoto, 1998). These data reveal a role for PTEN in controlling mitochondrial integrity and cell survival via PDHK1 regulation. When PDHK1 is inhibited in PTEN-deficient cells, multiple mechanisms contribute to cell death.

PDHK1 inhibition by DCA treatment also suppressed colony formation *in vitro* specifically in PTEN-deficient lung adenocarcinoma cells (Figure S5A) and tumor growth *in vivo* in PTEN-deficient melanoma xenograft models (Figure S5B). These data indicate PDHK1 is conditionally essential for survival specifically in PTEN-deficient cells and tumors.

PDHK1 Upregulation and Activation upon PTEN Loss Promotes Aerobic Glycolysis

We explored the functional consequences of PDHK1 upregulation induced by PTEN inactivation. PTEN and PDHK1 each can regulate energy metabolism but are not known to function together (Gottlob et al., 2001; Jang et al., 2013; Semenza, 2008). PDHK1 activation can promote aerobic glycolysis, through which pyruvate is converted to lactate to produce ATP, by phosphorylating and inactivating PDHA1 and blocking pyruvate entry into the TCA cycle (Patel et al., 2014). We investigated the metabolic effects of PDHK1 upregulation in cells with PTEN deficiency.

Silencing PTEN in cells induced L-lactate secretion, a hallmark of aerobic glycolysis (Figure S6A). PTEN-deficient cells exhibited a marked (4- to 5-fold) increase in L-lactate production in comparison with when these cells were grown in the presence of 2-DG (2-deoxyglucose, a glucose derivative that cannot undergo further glycolysis; Schulze and Harris, 2012;

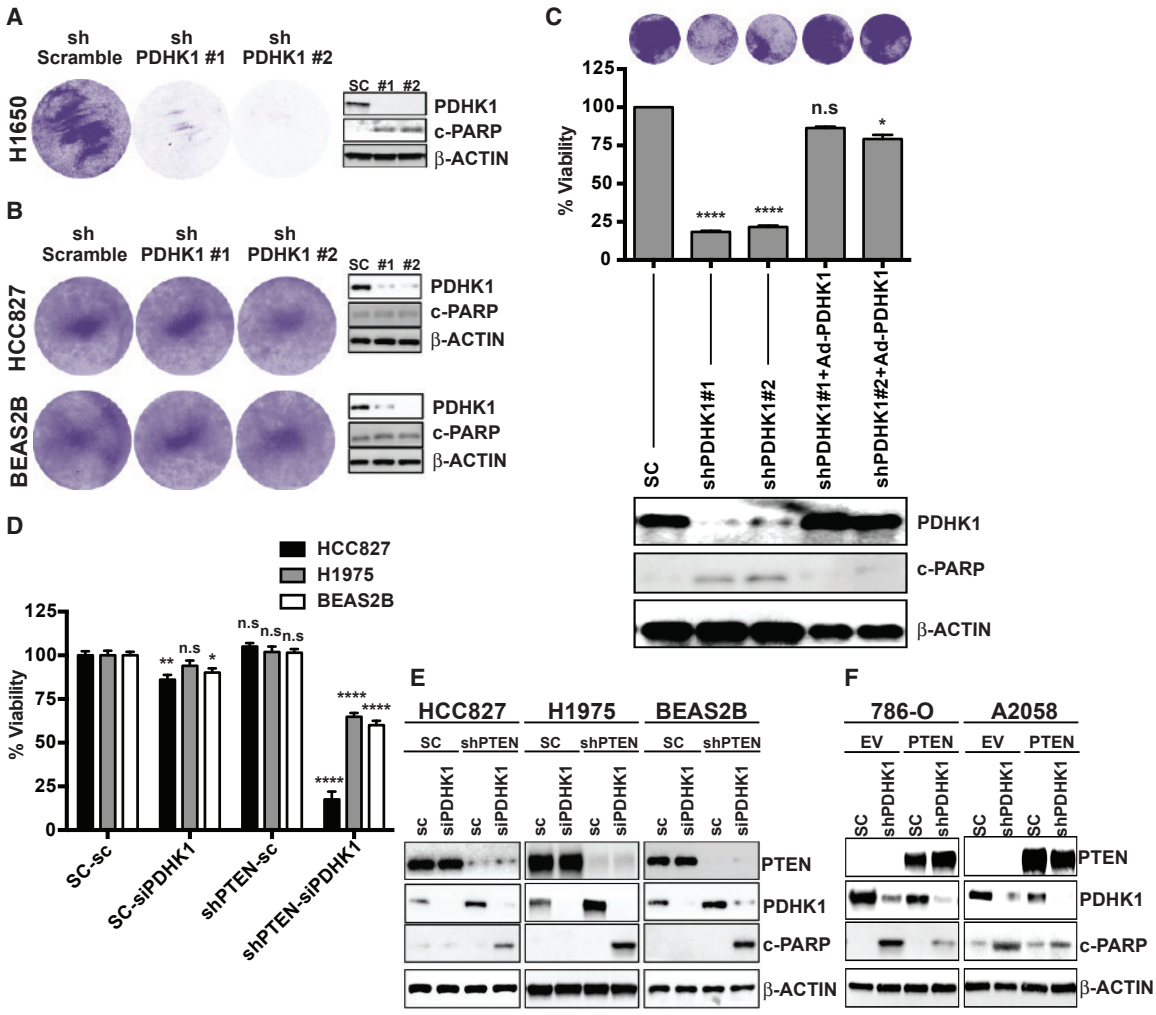

Figure 2. PTEN Loss or Inactivation Induces Cellular Dependence on PDHK1 for Survival

(A and B) Effects of stable PDHK1 knockdown in PTEN-deficient cancer (H1650) (A) or PTEN-proficient cancer (HCC827) and normal (Beas2B) cell lines (B) on cell growth by crystal violet staining assay (left) and apoptosis induction as measured by cleaved PARP levels by immunoblot analysis (right) are shown. shPDHK1#1 and shPDHK1#2, shRNAs to PDHK1; shScramble, scrambled control shRNA.

(C) Effects of stable PDHK1 knockdown and adenovirus-based shRNA resistant PDHK1 re-expression in PTEN-deficient H1650 cancer cells on cell growth by crystal violet staining assay (top) or CellTiter-Glo luminescent assay (middle) and apoptosis induction as measured by cleaved PARP levels by immunoblot analysis (bottom) are shown. shPDHK1#1 and shPDHK1#2, shRNAs to PDHK1; SC, scrambled control shRNA. Data are shown as mean ± SEM (n = 8 replicates). *$p < 0.05$ and ****$p < 0.0001$; n.s., not significant compared with "scrambled control shRNA expressing PTEN-deficient cells" by Dunn's multiple-comparisons one-way ANOVA.

(D and E) Effects of transient PDHK1 knockdown in PTEN-proficient cancer and normal cell lines with or without stable PTEN knockdown on cell viability by crystal violet staining assay (D) and apoptosis induction as measured by cleaved PARP levels by immunoblotting (E) are shown. siPDHK1, PDHK1 specific small interfering RNAs; sc, scrambled control siRNA; shPTEN, shRNA to PTEN; SC, scrambled control shRNA. Data are shown as mean ± SEM (n = 4 replicates). *$p < 0.05$, **$p < 0.01$, and ****$p < 0.0001$; n.s., not significant compared with "scrambled control siRNA and shRNA expressing PTEN-proficient cells" by Tukey's multiple-comparisons one-way ANOVA.

(F) Effects of stable PDHK1 knockdown in PTEN-deficient cancer cell lines stably expressing PTEN or empty vector (EV) on apoptosis induction as measured by cleaved PARP levels by immunoblotting are shown. shPDHK1, shRNA to PDHK1; SC, scrambled control shRNA.

See also Figures S3–S6.

Zhao et al., 2013) that suppresses lactate production independently (Figure S6B). PDHK1 suppression by shRNA or by DCA treatment or by stable PTEN re-expression in PTEN-deficient cell lines decreased L-lactate production (Figure S6B). These data suggest that PDHK1 upregulation and activation that occurs upon loss of PTEN promotes aerobic glycolysis in cells.

Treatment with rotenone (Palmer et al., 1968), an inhibitor of mitochondrial electron transport chain complex I (Figure S6C), or with oligomycin (Lardy et al., 1958), an inhibitor of mitochondrial ATP synthase (Figure S6D), resulted in greater inhibition of ATP production among PTEN-proficient cells but not PTEN-deficient cells. These data suggest that PTEN-deficient cells rely less

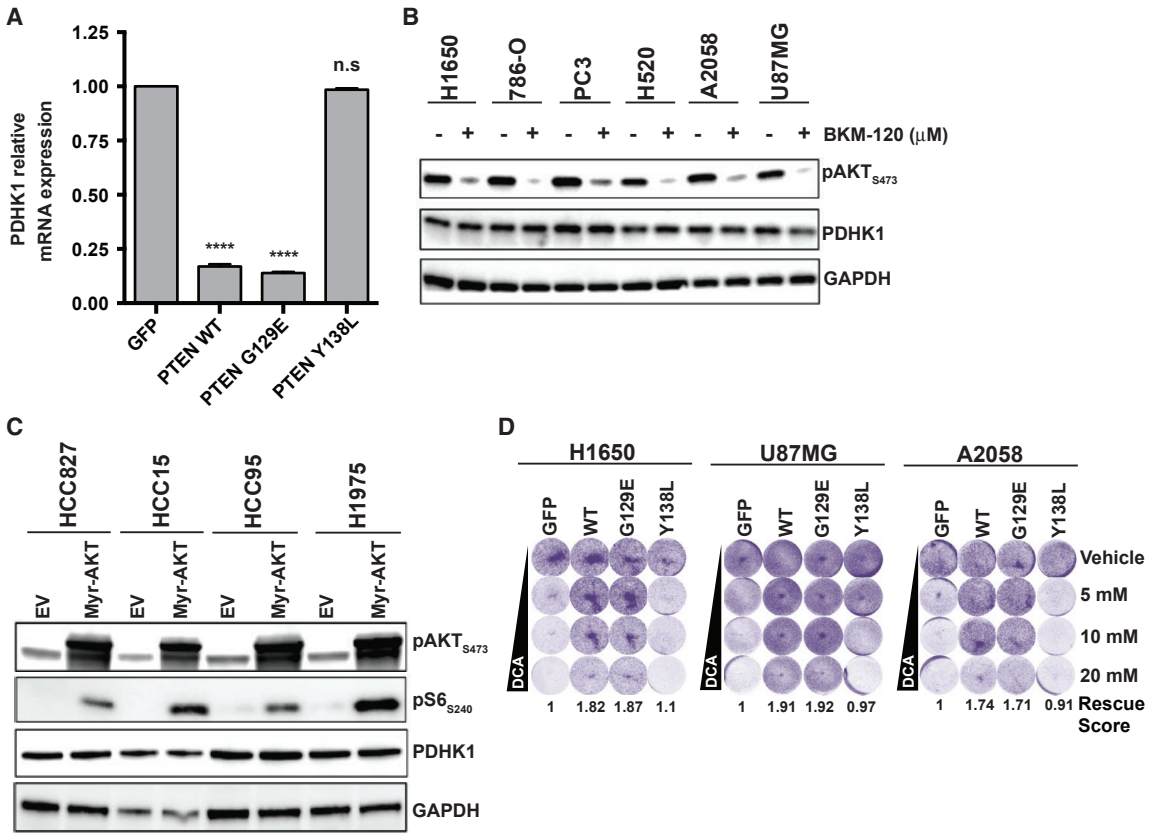

Figure 3. PTEN Protein Phosphatase Represses PDHK1 Independent of PI3K/AKT, and PTEN Protein Phosphatase Deficiency Renders PDHK1 Essential for Cell Survival

(A) Real-time qRT-PCR analysis of PDHK1 mRNA expression in PTEN-deficient A2058 cancer cells stably expressing $PTEN^{WT}$ or $PTEN^{G129E}$ or $PTEN^{Y138L}$ or GFP. Data are shown as mean ± SD (n = 2 replicates). ****p < 0.0001; n.s., not significant compared with "GFP-expressing PTEN-deficient cells" by Tukey's multiple-comparisons one-way ANOVA.

(B) Western blots showing phospho-AKT and PDHK1 expression in PTEN-deficient cancer cell lines in response to 1 μM BKM-120 (PI3-kinase inhibitor) or vehicle (DMSO) treatment for 24 h.

(C) Western blots showing phospho-AKT, phospho-S6 (mTOR effector), and PDHK1 expression in PTEN-proficient cancer cell lines expressing empty vector (EV) or myristoylated-AKT (Myr-AKT) to constitutively activate AKT signaling.

(D) Effects of pharmacologic inhibition of PDHK1 with DCA (dose response: 5, 10, and 20 mM) in PTEN-deficient cancer cell lines stably expressing $PTEN^{WT}$ or $PTEN^{G129E}$ or $PTEN^{Y138L}$ or GFP on cell growth by crystal violet staining assay are shown, with quantification of cell viability in 20 mM DCA treatment relative to vehicle (water) treatment reported as rescue score (STAR Methods).

See also Figure S7.

on oxidative phosphorylation for ATP production compared with PTEN-proficient cells.

Because increased PDHK1 promoted aerobic glycolysis in PTEN-deficient cells (Figure S6B), we tested whether PTEN inactivation enhances cellular glucose dependence, a hallmark of aerobic glycolysis (Lunt and Vander Heiden, 2011). The growth of PTEN-deficient but not PTEN-proficient cells was significantly decreased in glucose-deficient media, an effect rescued by stable PTEN expression (Figures S6E and S6F). These collective data indicate a metabolic shift toward aerobic glycolysis upon PTEN loss.

PTEN Protein Phosphatase Deficiency Activates PDHK1 Independent of PI3K/AKT and Induces Vulnerability to PDHK1 Inhibition

We next investigated the mechanism by which PTEN regulates PDHK1 expression. We determined the requirement of the distinct lipid and protein phosphatase activities of PTEN in the regulation of PDHK1. We leveraged established cancer-derived PTEN mutants that abrogate either PTEN's lipid phosphatase activity ($PTEN^{G129E}$) or its protein phosphatase activity ($PTEN^{Y138L}$) or both ($PTEN^{C124S}$) (Davidson et al., 2010; Myers et al., 1997, 1998; Rodríguez-Escudero et al., 2011; Tibarewal et al., 2012). By stably expressing each of these PTEN mutants or $PTEN^{WT}$ in a controlled system of PTEN-deficient cells, we found that the protein phosphatase, but not the lipid phosphatase, activity of PTEN regulates PDHK1 mRNA expression (Figure 3A). We confirmed that both mRNA and protein expression levels of PDHK1 were diminished upon expression of $PTEN^{WT}$ or the PTEN mutant that retains the protein phosphatase activity only ($PTEN^{G129E}$, lipid phosphatase mutant) in comparison with PTEN-deficient parental cells (Figures 3A and S7A). PDHK1 protein levels were unaffected by expression of the PTEN mutant

lacking both phosphatase activities (PTEN^{C124S}), suggesting that PDHK1 regulation by PTEN is phosphatase activity dependent and not via other non-enzymatic properties of PTEN (Freeman et al., 2003; Planchon et al., 2008; Shen et al., 2007) (Figure S7A).

Because PDHK1 levels were unaffected by the presence or absence of the PTEN lipid phosphatase, we investigated whether PDHK1 activation in PTEN-deficient cells was dependent upon PI3K/AKT signaling. Pharmacologic inhibition of PI3K or AKT in PTEN-deficient cells treated with BKM-120 (Burger et al., 2011) or MK2206 (Hirai et al., 2010), respectively, suppressed AKT activation (phospho-AKT levels) and expression of hexokinase 2 (HK2) (Figures S7B and S7C), which is upregulated in PTEN-deficient cells (Wang et al., 2014). In contrast, the expression of PDHK1 was unaffected under these conditions of PI3K/AKT blockade (Figures 3B and S7B–S7D).

AKT inactivates glycogen synthase kinase 3 α/β (GSK3α/β) through phosphorylation (Cross et al., 1995). Phospho-GSK3α/β levels were suppressed in PTEN-deficient cell lines by BKM-120 treatment, confirming the efficacy of the inhibitor; PDHK1 expression was not significantly affected (Figure S7D). Treatment with BKM-120 (Burger et al., 2011) and another PI3K inhibitor, GDC0941 (Folkes et al., 2008), suppressed phosphorylation of ribosomal protein S6, which is downstream of both AKT and mTORC1, in three different PTEN-deficient cell lines tested and consistent with prior studies (Neshat et al., 2001), without decreasing PDHK1 levels (Figures S7D and S7E).

Ectopic expression of a constitutively active form of AKT (Myr-AKT) (Fulton et al., 1999; Sun et al., 2014), while increasing phospho-S6 levels (Wittenberg et al., 2016), did not increase PDHK1 levels in PTEN-expressing cells (Figure 3C). Thus, PDHK1 is upregulated specifically by PTEN protein phosphatase inactivation, and in a PI3K/AKT-independent manner.

We further found that it was the protein phosphatase, but not the lipid phosphatase, activity of PTEN that was required to rescue PTEN-deficient cells from the lethal effects of PDHK1 inhibition (Figure 3D). These collective data indicate that PDHK1 is conditionally essential for the survival of specifically PTEN protein phosphatase-deficient cells.

PTEN Protein Phosphatase Suppresses Nuclear Factor κB (NF-κB) Activation to Repress PDHK1

We next investigated the mechanism by which PTEN protein phosphatase inactivation increases PDHK1 gene (and thus protein) expression. Although PDHK1 expression can be upregulated by the transcription factor hypoxia-inducible factor 1 (HIF-1) (Kim et al., 2006), silencing the HIF-1α subunit of HIF-1 failed to suppress PDHK1 expression in a panel of PTEN-deficient cell lines, unlike the effects of HIF-1α silencing in these cells on carbonic anhydrase 9 (CA9), which is known to be regulated by HIF-1 (Figure S8A) (Wykoff et al., 2000). Although we observed HIF-1 independency on PDHK1 induction in PTEN-null cell lines under normoxia (Figure S8A), PTEN deficiency further increased PDHK1 expression in hypoxic conditions concurrently with HIF-1 induction, compared with normoxia (Figure S8B).

To understand the molecular basis of the transcriptional upregulation of PDHK1 induced by PTEN inactivation in cells, we sought to identify the transcription factor(s) involved. We analyzed putative transcription factor binding sequences and/or motifs in or upstream of the PDHK1 promoter using an *in silico* promoter analysis. We identified a putative nuclear factor kappa light chain enhancer of activated B cells (NF-κB) transcription factor (Gilmore, 2006) consensus DNA binding site (GGGRNNYYCC; R is purine, Y is pyrimidine, and N is any base) (Martone et al., 2003) GGGACGCTCC at nucleotide position 173420479 in chromosome 2, at ~300 bp upstream of the TSS (transcription start site) in the PDHK1 promoter (Figures 4A and S8C; Table S3). We tested the hypothesis that PDHK1 is a transcriptional target of the transcription factor NF-κB.

We found NF-κB transcription factor RELA (p65) subunit recruitment at the PDHK1 promoter in multiple PTEN-deficient cancer cell types by chromatin immunoprecipitation (ChIP) and real-time qPCR analysis (Figure 4A). NF-κB suppression using either an shRNA to knockdown RELA or the established NF-κB small-molecule inhibitor PBS-1086 (Blakely et al., 2015; Fabre et al., 2012) inhibited NF-κB, decreased PDHK1 expression, and suppressed phosphorylation of the PDHK1 protein substrate PDHA1 in a panel of PTEN-deficient cell lines (Figures 4B and S8D). Although prior studies have shown that PTEN loss and consequent AKT activation can activate NF-κB (Chiao and Ling, 2011; Dan et al., 2008; Gustin et al., 2001; Koul et al., 2001; Mayo et al., 2002), our data reveal that NF-κB hyperactivation upon PTEN loss promotes PDHK1 expression and establish PDHK1 as a NF-κB target gene.

NF-κB inhibitor treatment (Blakely et al., 2015; Fabre et al., 2012) decreased cell survival specifically in PTEN-deficient cells (Figure S8E), phenocopying the effects of PDHK1 inhibition (Figure 2). Thus, PTEN loss renders cells dependent on PDHK1 for survival via NF-κB activation. Stable expression of PDHK1 in PTEN-deficient A2058 (melanoma) cells partially rescued loss of cell viability and decreased apoptosis upon NF-κB inhibition (with Bay 11-7085; Berger et al., 2007) (Figures S8F and S8G).

Both the lipid, as expected (Gustin et al., 2001), and protein phosphatase activities of PTEN decreased NF-κB transcriptional activity (Aoki and Kao, 1997; Blakely et al., 2015) and NF-κB nuclear localization (Figures 4C and 4D). However, although the lipid phosphatase activity of PTEN specifically suppressed AKT activation (phospho-AKT levels), as expected (Gustin et al., 2001), the protein phosphatase activity of PTEN was specifically required to suppress PDHK1 expression via decreased NF-κB activation (phospho-RELA levels) (Figure 4E). Thus, although both the lipid and protein phosphatase activities of PTEN regulate NF-κB, the expression of PDHK1 is regulated predominantly by the protein phosphatase activity of PTEN via NF-κB.

PTEN Protein Phosphatase Regulates NF-κB and PDHK1 via NKAP

We investigated how the PTEN protein phosphatase regulates its downstream effectors NF-κB and PDHK1. De-phosphorylation of a specific protein target of the PTEN protein phosphatase activity could link PTEN to downstream NF-κB and PDHK1 regulation. The full compendium of PTEN protein or lipid phosphatase specific effectors and substrates remains incompletely characterized. To identify the potential PTEN protein phosphatase-specific effector that links PTEN to downstream NF-κB

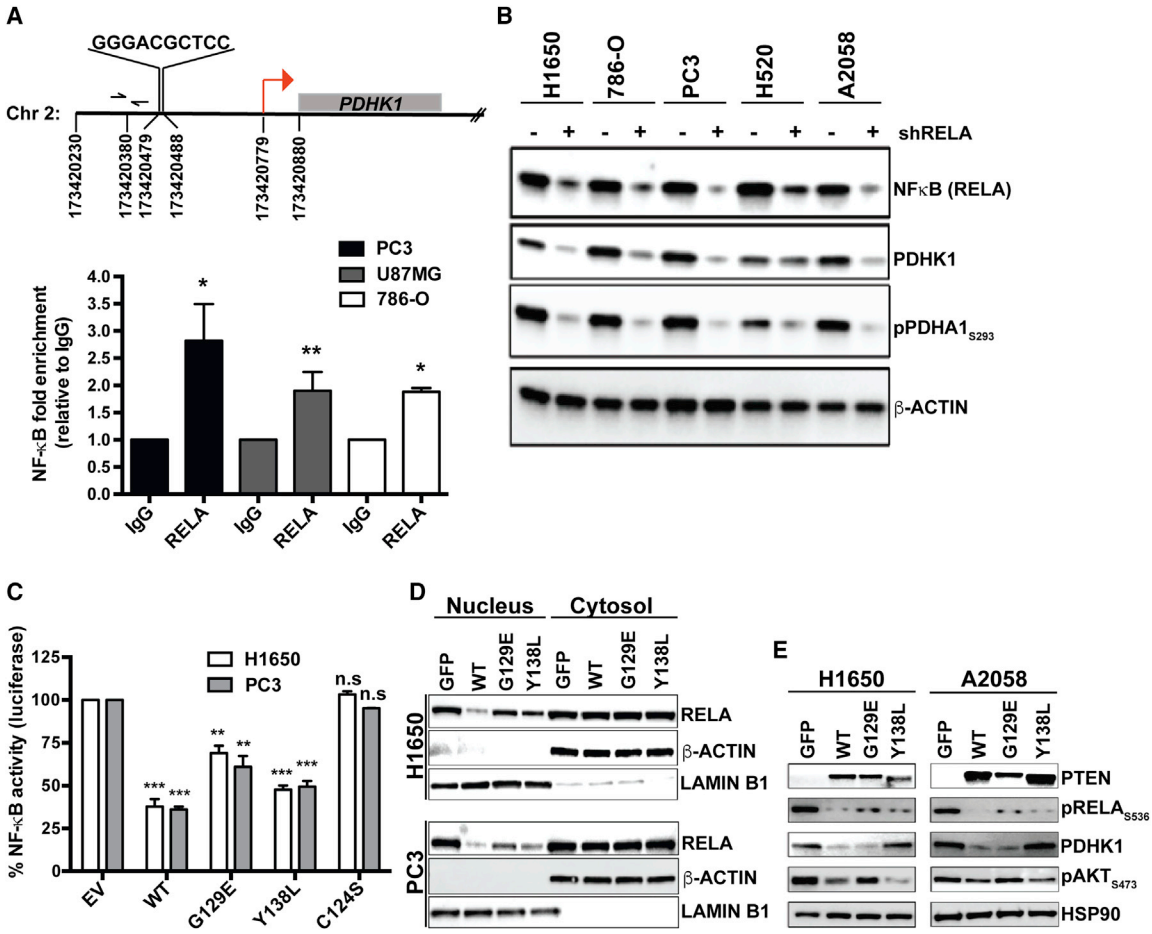

Figure 4. PTEN Protein Phosphatase Represses PDHK1 by Suppressing NF-κB Activation

(A) Top: identification of NF-κB consensus binding site in the promoter of PDHK1 gene located between nucleotide positions 173420479 and 173420488 in chromosome 2, ~300 bp upstream of the transcription start site (TSS; red arrow) at nucleotide position 173420779. Bottom: NF-κB (RELA) recruitment at PDHK1 promoter in PTEN-deficient cancer cells by ChIP assay. Primers (forward and reverse arrows) used to amplify a 118 bp region (spanning nucleotide position 173420380) ~40 bp upstream of the NF-κB binding site in the PDHK1 promoter are shown. Fold enrichment (RELA ChIP DNA [pg] to IgG DNA [pg]) data are shown as mean ± SEM (n = 3 replicates). *$p < 0.05$ and **$p < 0.01$ compared with "IgG control" by two-tailed unpaired t test with Welch's correction.

(B) Western blots showing NF-κB (RELA), PDHK1, and phospho-PDHA1 expression in PTEN-deficient cancer cell lines with or without stable RELA knockdown. shRELA, shRNA to RELA.

(C) Effects of $PTEN^{WT}$ or $PTEN^{G129E}$ or $PTEN^{Y138L}$ or empty vector (EV) expression in PTEN-deficient cancer cell lines on NF-κB activity by luciferase reporter assays (STAR Methods) are shown. Data are shown as mean ± SD (n = 2 replicates). **$p < 0.01$ and ***$p < 0.001$ compared with "empty vector control expressing PTEN-deficient cells" by Tukey's multiple-comparisons one-way ANOVA.

(D) Effects of $PTEN^{WT}$ or $PTEN^{G129E}$ or $PTEN^{Y138L}$ or GFP expression in PTEN-deficient cancer cell lines on NF-κB (RELA) subcellular localization by nuclear-cytoplasmic fractionation and immunoblotting are shown. Western blots were also probed with anti-LaminB1 and anti-actin β antibodies as nuclear and cytoplasmic markers, respectively.

(E) Western blots showing PTEN, phospho-RELA, PDHK1, and phospho-AKT expression in PTEN-deficient cancer cell lines stably expressing $PTEN^{WT}$, $PTEN^{G129E}$, $PTEN^{138L}$, or GFP.

See also Figure S8 and Table S3.

and PDHK1 regulation, we used global mass spectrometry-based phospho-proteomics profiling (Beltrao et al., 2012; Jäger et al., 2011) in a genetically controlled system of PTEN-deficient cell lines with stable GFP or $PTEN^{WT}$ or $PTEN^{G129E}$ (lipid phosphatase mutant) or $PTEN^{Y138L}$ (protein phosphatase mutant) re-expression (Figure 5A). We identified phospho-peptides and proteins significantly differentially regulated (log_2 fold change < -0.5, $q < 0.05$) by each PTEN phosphatase activity, in comparison with PTEN-null GFP-expressing control cells (Figure 5A). We prioritized the phospho-proteins that exhibited conserved and specific regulation by the PTEN protein-phosphatase activity in both H1650 (lung adenocarcinoma, EGFR mutant) and A2058 (melanoma, BRAF mutant) cells. The different tissue type and genetic background of these two cell lines provided a filter to identify a potentially conserved target. Forty-two proteins exhibited PTEN protein phosphatase-specific

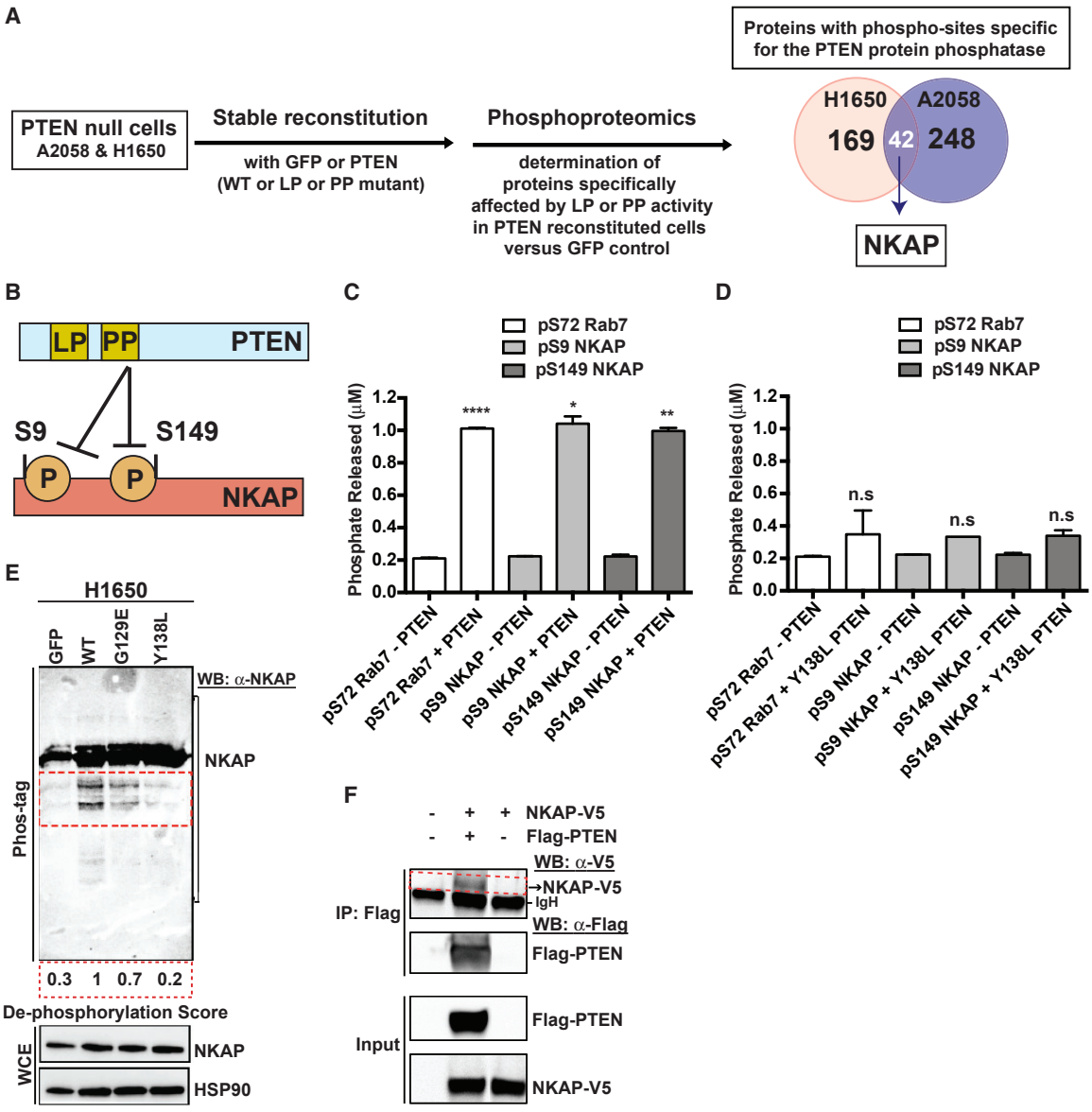

Figure 5. PTEN Dephosphorylates NF-κB-Activating Protein (NKAP)

(A) Left: workflow of the unbiased, global phospho-proteomic profiling in PTEN-deficient cancer cell lines stably expressing $PTEN^{WT}$ or $PTEN^{G129E}$ or $PTEN^{Y138L}$ or GFP to identify the phospho-peptides (and corresponding proteins) affected specifically by the protein or lipid phosphatase (PP or LP) activity of PTEN. Right: Venn diagram showing the number of proteins with phospho-sites specifically affected by the protein phosphatase activity of PTEN in H1650 (n = 169) and A2058 (n = 248) cells, with the phospho-proteins (including NF-κB-activating protein, NKAP highlighted in white) affected in both cell lines shown in the overlap (n = 42).

(B) Schematic representation of NKAP phospho-sites at serines 9 and 149 affected by the protein phosphatase activity of PTEN.

(C and D) Phosphate released (μM) from a phospho-S9-NKAP or phospho-S149-NKAP or phospho-S72-Rab7 (control) peptide after incubation without or with recombinant WT PTEN (C) or protein phosphatase mutant Y138L PTEN (D) enzyme in an *in vitro* malachite green-based colorimetric assay. Data are shown as mean ± SD (n = 2 replicates). *$p < 0.05$, **$p < 0.01$, and ****$p < 0.0001$ compared with "no PTEN" control by two-tailed unpaired t test with Welch's correction.

(E) Detection of phospho-NKAP and its de-phosphorylated species (indicated by the red dotted inset) in PTEN-deficient cancer cell lines stably expressing either $PTEN^{WT}$ or $PTEN^{G129E}$ or $PTEN^{Y138L}$ or GFP by Phos-tag PAGE and immunoblotting. De-phosphorylation score indicates the extent to which expression of each PTEN mutant in PTEN-deficient cells suppresses NKAP de-phosphorylation relative to $PTEN^{WT}$ (set at 1). A lower de-phosphorylation score indicates less de-phosphorylation of NKAP.

(F) Co-immunoprecipitation of NKAP (indicated by the red dotted inset) with PTEN upon overexpression of both NKAP-V5 and FLAG-PTEN and not NKAP-V5 overexpression alone or no overexpression in 293T cells followed by IP-FLAG is shown. Arrowhead denotes NKAP-V5, while the dark band below is background due to secondary antibody cross-reactivity to the immunoglobulin heavy chain (IgH) used in IP.

See also Figure S9.

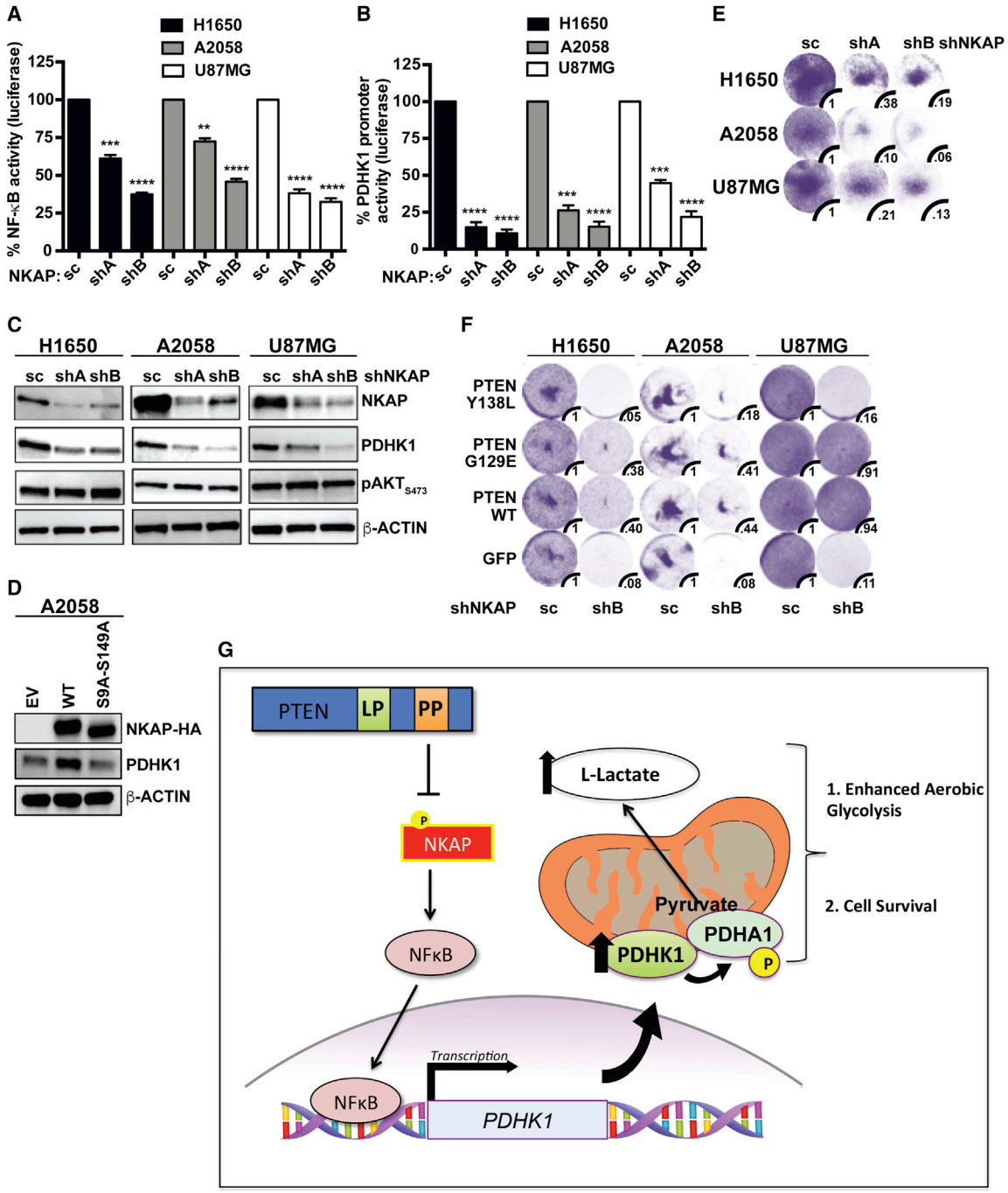

Figure 6. Depletion of NKAP Decreases NF-κB Activation and PDHK1 Expression and Induces Synthetic Lethality Specifically upon PTEN Protein Phosphatase Loss

(A and B) Effects of stable NKAP knockdown in PTEN-deficient cancer cell lines on NF-κB activity (A) or PDHK1 promoter activation (B) by luciferase reporter assays (STAR Methods) are shown. shA and shB, shRNAs to NKAP; SC, scrambled control shRNA. Data are shown as mean ± SEM (n = 3 replicates). **p < 0.01, ***p < 0.001, and ****p < 0.0001 compared with "scrambled control shRNA expressing PTEN-deficient cells" by Tukey's multiple-comparisons one-way ANOVA.

(C) Western blots showing NKAP, PDHK1, and phospho-AKT expression in PTEN-deficient cancer cell lines with or without stable NKAP knockdown. shA and shB, shRNAs to NKAP; SC, scrambled control shRNA.

(D) Western blots showing HA-NKAP and PDHK1 expression in PTEN-deficient A2058 cancer cells stably expressing empty vector (EV) or wild-type NKAP (HA-NKAP^{WT}) or de-phosphorylation-deficient mutant NKAP (HA-NKAP$^{S9A-S149A}$).

(E and F) Effects of stable NKAP knockdown in PTEN-deficient cancer cell lines without (E) or with stable PTEN^{WT} or PTEN^{G129E} or PTEN^{Y138L} or GFP expression (F) on cell growth by crystal violet staining assay are shown, with quantification of cell viability under each condition relative to cells expressing the scrambled control shRNA. shA and shB, shRNAs to NKAP; SC, scrambled control shRNA.

(legend continued on next page)

regulation in both cell lines, including NF-κB-activating protein (NKAP) (Figures 5A and S9A).

NKAP, originally identified as a regulator of NF-κB activation (Chen et al., 2003), has various cellular functions (Pajerowski et al., 2009; Thapa et al., 2016; Burgute et al., 2014; Li et al., 2016). NKAP is not known to be linked to PTEN or the regulation of cellular metabolism or cancer. Given NKAP's established ability to activate NF-κB (Chen et al., 2003), which regulates PDHK1 expression (Figure 4), NKAP was prioritized as a prime candidate PTEN effector arising from our phospho-proteomics screen (Figures 5A and S9A).

We examined whether NKAP is a phospho-protein target of PTEN in biochemical assays. The phospho-proteomics profiling revealed the predominant phosphorylation sites in NKAP in the two cell lines tested were at serines 9 and 149 (Figures 5B and S9A), consistent with other protein phospho-site mapping data (available at phosphosite.org). Using Ser 9 or Ser 149 phosphorylated NKAP peptides in an established malachite green-based *in vitro* phosphatase assay with recombinant $PTEN^{WT}$ and $PTEN^{Y138L}$ enzymes (Figures 5C and 5D), we found that WT PTEN ($PTEN^{WT}$) enzyme de-phosphorylated NKAP at serines 9 and 149 with similar efficiency (as quantified by the amount of Pi released) as a known phospho-serine substrate of PTEN, phospho-S72 Rab7 (Shinde and Maddika, 2016), used as a positive control (Figure 5C). The protein phosphatase defective PTEN ($PTEN^{Y138L}$) enzyme had little or no activity for either phospho-NKAP or phospho-Rab7 and was comparable with the "no enzyme" control (Figure 5D).

By phosphate affinity (Phos-tag) PAGE analysis (Kinoshita et al., 2009), wherein de-phosphorylated NKAP migrates faster than its phosphorylated form, we found enhanced NKAP dephosphorylation in PTEN-deficient cells stably expressing $PTEN^{WT}$ or $PTEN^{G129E}$ (lipid phosphatase mutant) in comparison with those with stable $PTEN^{Y138L}$ (protein phosphatase mutant) or GFP expression (Figure 5E). These cellular Phos-tag assays independently confirmed that the protein phosphatase activity of PTEN predominantly regulates NKAP phosphorylation. We noted no significant effect of PTEN re-expression on NKAP protein levels in PTEN-deficient cells (Figure 5E), suggesting that PTEN primarily regulates NKAP phosphorylation and not its expression. No effect of PTEN expression on PDHK1 phosphorylation was observed (Figure S9A), suggesting that although PTEN regulates PDHK1 gene expression via NF-κB, it does not dephosphorylate PDHK1 protein.

NKAP co-immunoprecipitated with PTEN when overexpressed in 293T cells (Figure 5F, red box) under identical conditions in which the known PTEN interactor NHERF2 (Takahashi et al., 2006) was co-immunoprecipitated with PTEN (Figure S9B). An independent affinity purification-mass spectrometry analysis (St-Denis et al., 2016) provided evidence for this PTEN-NKAP interaction in cells. These data reveal NKAP as a protein interactor of PTEN and that PTEN dephosphorylates NKAP at two conserved serine residues, S9 and S149.

To further investigate whether NKAP is a molecular link between PTEN and PDHK1, we examined whether NF-κB activation and PDHK1 expression are suppressed by silencing NKAP in PTEN-deficient cells. NKAP knockdown in different PTEN-deficient cell lines suppressed NF-κB transcriptional activity (Aoki and Kao, 1997; Blakely et al., 2015) (Figure 6A) without affecting phospho-AKT levels (Figure 6C), consistent with prior work (Thapa et al., 2016). In concordance, NKAP knockdown suppressed transcriptional activation of the PDHK1 promoter (Figure 6B) and decreased expression of PDHK1 (Figure 6C), which we identified as a NF-κB target gene (Figure 4). Stable expression of WT NKAP ($NKAP^{WT}$), but not de-phosphorylation-deficient mutant NKAP ($NKAP^{S9A-S149A}$), in PTEN-null cells enhanced NF-κB transcriptional activity (Figure S10A) and NF-κB nuclear localization (Figure S10B) and increased PDHK1 expression (Figure 6D). Thus, loss of the PTEN protein phosphatase induces NKAP phosphorylation (on S9 and S149) to activate NF-κB and increase PDHK1 levels, in a PI3K-AKT-independent manner.

We propose that specific loss of the PTEN protein phosphatase activates a downstream NKAP-NF-κB signaling axis to drive PDHK1 expression and cellular dependence on PDHK1 for survival (Figure 6G). NKAP knockdown significantly decreased cell viability in PTEN-deficient cells compared with PTEN-expressing cells (Figure 6E), phenocopying the effects of both PDHK1 and NF-κB inhibition in PTEN-deficient cells (Figures 2, S4, and S8C). Similar to PDHK1 inhibition (Figure 3D), NKAP silencing significantly decreased the viability of cells specifically lacking the PTEN protein phosphatase activity (Figure 6F). NKAP silencing affected viability of cells expressing $PTEN^{WT}$ or $PTEN^{G129E}$ to some extent which may be due to other effects of NKAP knockdown. PTEN-deficient cells re-constituted with $PTEN^{Y138L}$ (protein phosphatase mutant) were generally as sensitive as PTEN-deficient cells to NKAP knockdown (Figure 6F). In contrast, cells re-constituted with PTEN that harbors the protein phosphatase activity (either $PTEN^{WT}$ or $PTEN^{G129E}$, the lipid phosphatase mutant) were generally less affected by NKAP suppression (Figure 6F). These data show a role for the PTEN protein phosphatase in controlling cell survival via regulation of a PTEN/NKAP/NF-κB/PDHK1 signaling axis.

DISCUSSION

Our findings unveil molecular events specifically regulated by the protein phosphatase activity of PTEN in mammalian cells and cancer and uncover a vulnerability in PTEN-deficient cancers (i.e., PDHK1 dependence; Figure 6G). Our findings highlight PDHK1 as a promising therapeutic target for evaluation for improving the treatment of PTEN-deficient cancers, an unmet clinical need. Our study illustrates the importance of defining activity-specific PTEN functions that contribute to physiologic regulation in normal cells and that when dysregulated contribute to genetically driven human diseases such as cancer.

Our data suggest that PTEN's different enzymatic activities can be used by cells to impart specificity in the regulation of

(G) Model of cellular survival and energy metabolism regulation specifically by the protein-phosphatase activity of PTEN via a NKAP-NF-κB-PDHK1-driven signaling axis. Loss of the PTEN protein-phosphatase activity promotes NKAP phosphorylation, NF-κB activation, and PDHK1 upregulation, thereby enhancing aerobic glycolysis and rendering PTEN protein-phosphatase deficient cells dependent on NKAP and PDHK1 for survival.
See also Figure S10.

cell signaling and transcriptional output (here, via NKAP/NF-κB/PDHK1). The differential recruitment of NF-κB to genomic loci such as the PDHK1 promoter may be guided not only by the underlying DNA sequence in canonical gene regulatory elements, but also by co-factor proteins that influence preferential recruitment of NF-κB to one target gene promoter or another. Different co-factor proteins can regulate NF-κB binding at specific target genes under certain conditions (Wan and Lenardo, 2009). NKAP may act as a co-factor specifically regulated by the PTEN protein phosphatase activity to direct differential NF-κB target promoter binding and gene expression only upon loss of the PTEN protein phosphatase. This model may help explain how cells finely tune NF-κB's broad transcriptional repertoire via activity-specific upstream inputs, such as the bi-functional phosphatase PTEN.

STAR★METHODS

Detailed methods are provided in the online version of this paper and include the following:

- KEY RESOURCES TABLE
- LEAD CONTACT AND MATERIALS AVAILABILITY
- EXPERIMENTAL MODEL AND SUBJECT DETAILS
  - Animals
  - Cell cultures
- METHOD DETAILS
  - Transfection and viral infection
  - Cell viability and growth assays
  - Intracellular ATP and ROS measurement
  - L-lactate measurement
  - Protein blot analysis
  - Gene expression profiling
  - Real time qRT-PCR
  - Chromatin immunoprecipitation (ChIP) assays
  - Luciferase reporter assays
  - *In vitro* phosphatase assays
  - Phos-tag assays
  - Immunoprecipitation
  - Time-lapse imaging
  - Immunohistochemistry
  - Phospho-proteomics study
  - Colony formation assays
  - Animal studies
- QUANTIFICATION AND STATISTICAL ANALYSIS
  - Statistical analyses
  - TCGA data analysis
  - Gene expression array data analysis
  - Phospho-proteomics Data Analysis
- DATA AND CODE AVAILABILITY

SUPPLEMENTAL INFORMATION

Supplemental Information can be found online at https://doi.org/10.1016/j.celrep.2019.07.063.

ACKNOWLEDGMENTS

We would like to thank all members of the Bivona laboratory for critical review of the manuscript and acknowledge funding support from NIH/NCI grants U54CA224081, R01CA204302, R01CA211052, and R01CA169338 and the Pew Foundation and Stewart Foundation (to T.G.B.); U54 CA209891 (to N.J.K.); R01GM123159 (to J.S.F.); R01GM118939 (to Y.K.); and NIH/NCI T32CA108462-14 (to N.C.). We thank Timothy Fouts and Jeffrey Meshulam at Profectus Biosciences, Inc., for generously providing PBS-1086. We thank Bhagyashri Burgute and Angelika Noegel at the University of Cologne, Germany, for kindly providing the NKAP mouse mAb (K85-80-5). We thank Albertas Navickas and Hani Goodarzi at UCSF for the hypoxia chamber.

AUTHOR CONTRIBUTIONS

N.C., E.P., and T.G.B. conceived and designed the experiments and analyzed the data. N.C., E.P., M.K.M., P.G., D.V.A., G.H., V.O., J.J.Y., L.L., C.H.E., J.F., and E.C. performed the experiments. S.A. and W.W. analyzed microarray data. T.I., M.H. and W.A.W. analyzed TCGA tumor data. J.S. performed time-lapse microscopy and analyzed the data. B.A.B. helped N.C. with PTEN purification. E.V., J.R.J., B.W.N., J.V.D., and N.J.K. performed phospho-proteomics screen and analyzed the data. N.C., E.P., A.J.S., and T.G.B. wrote the manuscript with input from all authors.

DECLARATION OF INTERESTS

T.G.B. is an advisor to Array Biopharma, Revolution Medicines, Novartis, AstraZeneca, Takeda, Springworks, and Jazz Pharmaceuticals and receives research funding from Novartis and Revolution Medicines.

Received: October 22, 2018
Revised: June 19, 2019
Accepted: July 18, 2019
Published: August 27, 2019

SUPPORTING CITATIONS

The following references appear in the Supplemental Information: Millán-Uclés et al. (2016); Soria et al. (2002); Sun (2010); Tristan et al. (2011); Tsunoda and Takagi (1999).

REFERENCES

Aguissa-Touré, A.H., and Li, G. (2012). Genetic alterations of PTEN in human melanoma. Cell. Mol. Life Sci. *69*, 1475–1491.

Aoki, Y., and Kao, P.N. (1997). Cyclosporin A-sensitive calcium signaling represses NFkappaB activation in human bronchial epithelial cells and enhances NFkappaB activation in Jurkat T-cells. Biochem. Biophys. Res. Commun. *234*, 424–431.

Beltrao, P., Albanèse, V., Kenner, L.R., Swaney, D.L., Burlingame, A., Villén, J., Lim, W.A., Fraser, J.S., Frydman, J., and Krogan, N.J. (2012). Systematic functional prioritization of protein posttranslational modifications. Cell *150*, 413–425.

Berger, N., Ben Bassat, H., Klein, B.Y., and Laskov, R. (2007). Cytotoxicity of NF-kappaB inhibitors Bay 11-7085 and caffeic acid phenethyl ester to Ramos and other human B-lymphoma cell lines. Exp. Hematol. *35*, 1495–1509.

Blakely, C.M., Pazarentzos, E., Olivas, V., Asthana, S., Yan, J.J., Tan, I., Hrustanovic, G., Chan, E., Lin, L., Neel, D.S., et al. (2015). NF-κB-activating complex engaged in response to EGFR oncogene inhibition drives tumor cell survival and residual disease in lung cancer. Cell Rep. *11*, 98–110.

Bonnet, S., Archer, S.L., Allalunis-Turner, J., Haromy, A., Beaulieu, C., Thompson, R., Lee, C.T., Lopaschuk, G.D., Puttagunta, L., Bonnet, S., et al. (2007). A mitochondria-K+ channel axis is suppressed in cancer and its normalization promotes apoptosis and inhibits cancer growth. Cancer Cell *11*, 37–51.

Burger, M.T., Pecchi, S., Wagman, A., Ni, Z.J., Knapp, M., Hendrickson, T., Atallah, G., Pfister, K., Zhang, Y., Bartulis, S., et al. (2011). Identification of NVP-BKM120 as a potent, selective, orally bioavailable class I PI3 kinase inhibitor for treating cancer. ACS Med. Chem. Lett. *2*, 774–779.

Burgute, B.D., Peche, V.S., Steckelberg, A.L., Glöckner, G., Gaßen, B., Gehring, N.H., and Noegel, A.A. (2014). NKAP is a novel RS-related protein that interacts with RNA and RNA binding proteins. Nucleic Acids Res. *42*, 3177–3193.

Chalhoub, N., and Baker, S.J. (2009). PTEN and the PI3-kinase pathway in cancer. Annu. Rev. Pathol. *4*, 127–150.

Chandarlapaty, S., Sawai, A., Scaltriti, M., Rodrik-Outmezguine, V., Grbovic-Huezo, O., Serra, V., Majumder, P.K., Baselga, J., and Rosen, N. (2011). AKT inhibition relieves feedback suppression of receptor tyrosine kinase expression and activity. Cancer Cell *19*, 58–71.

Chen, D., Li, Z., Yang, Q., Zhang, J., Zhai, Z., and Shu, H.B. (2003). Identification of a nuclear protein that promotes NF-kappaB activation. Biochem. Biophys. Res. Commun. *310*, 720–724.

Chesney, J., Clark, J., Klarer, A.C., Imbert-Fernandez, Y., Lane, A.N., and Telang, S. (2014). Fructose-2,6-bisphosphate synthesis by 6-phosphofructo-2-kinase/fructose-2,6-bisphosphatase 4 (PFKFB4) is required for the glycolytic response to hypoxia and tumor growth. Oncotarget *5*, 6670–6686.

Chiao, P.J., and Ling, J. (2011). Kras, Pten, NF-κB, and inflammation: dangerous liaisons. Cancer Discov. *1*, 103–105.

Chinnaiyan, A.M., Orth, K., O'Rourke, K., Duan, H., Poirier, G.G., and Dixit, V.M. (1996). Molecular ordering of the cell death pathway. Bcl-2 and Bcl-xL function upstream of the CED-3-like apoptotic proteases. J. Biol. Chem. *271*, 4573–4576.

Choi, M., Chang, C.Y., Clough, T., Broudy, D., Killeen, T., MacLean, B., and Vitek, O. (2014). MSstats: an R package for statistical analysis of quantitative mass spectrometry-based proteomic experiments. Bioinformatics *30*, 2524–2526.

Cross, D.A., Alessi, D.R., Cohen, P., Andjelkovich, M., and Hemmings, B.A. (1995). Inhibition of glycogen synthase kinase-3 by insulin mediated by protein kinase B. Nature *378*, 785–789.

Dan, H.C., Cooper, M.J., Cogswell, P.C., Duncan, J.A., Ting, J.P., and Baldwin, A.S. (2008). Akt-dependent regulation of NF-kappaB is controlled by mTOR and Raptor in association with IKK. Genes Dev. *22*, 1490–1500.

Davidson, L., Maccario, H., Perera, N.M., Yang, X., Spinelli, L., Tibarewal, P., Glancy, B., Gray, A., Weijer, C.J., Downes, C.P., and Leslie, N.R. (2010). Suppression of cellular proliferation and invasion by the concerted lipid and protein phosphatase activities of PTEN. Oncogene *29*, 687–697.

Dey, N., Crosswell, H.E., De, P., Parsons, R., Peng, Q., Su, J.D., and Durden, D.L. (2008). The protein phosphatase activity of PTEN regulates SRC family kinases and controls glioma migration. Cancer Res. *68*, 1862–1871.

Fabre, C., Mimura, N., Bobb, K., Kong, S.Y., Gorgun, G., Cirstea, D., Hu, Y., Minami, J., Ohguchi, H., Zhang, J., et al. (2012). Dual inhibition of canonical and noncanonical NF-kappaB pathways demonstrates significant antitumor activities in multiple myeloma. Clin. Cancer Res. *18*, 4669–4681.

Figueiredo, A.L., Maczkowiak, F., Borday, C., Pla, P., Sittewelle, M., Pegoraro, C., and Monsoro-Burq, A.H. (2017). PFKFB4 control of AKT signaling is essential for premigratory and migratory neural crest formation. Development *144*, 4183–4194.

Folkes, A.J., Ahmadi, K., Alderton, W.K., Alix, S., Baker, S.J., Box, G., Chuckowree, I.S., Clarke, P.A., Depledge, P., Eccles, S.A., et al. (2008). The identification of 2-(1H-indazol-4-yl)-6-(4-methanesulfonyl-piperazin-1-ylmethyl)-4-morpholin-4-yl-thieno[3,2-d]pyrimidine (GDC-0941) as a potent, selective, orally bioavailable inhibitor of class I PI3 kinase for the treatment of cancer. J. Med. Chem. *51*, 5522–5532.

Freeman, D.J., Li, A.G., Wei, G., Li, H.H., Kertesz, N., Lesche, R., Whale, A.D., Martinez-Diaz, H., Rozengurt, N., Cardiff, R.D., et al. (2003). PTEN tumor suppressor regulates p53 protein levels and activity through phosphatase-dependent and -independent mechanisms. Cancer Cell *3*, 117–130.

Fulton, D., Gratton, J.P., McCabe, T.J., Fontana, J., Fujio, Y., Walsh, K., Franke, T.F., Papapetropoulos, A., and Sessa, W.C. (1999). Regulation of endothelium-derived nitric oxide production by the protein kinase Akt. Nature *399*, 597–601.

Ghosh, S., Varela, L., Sood, A., Park, B.H., and Lotan, T.L. (2013). mTOR signaling feedback modulates mammary epithelial differentiation and restrains invasion downstream of PTEN loss. Cancer Res. *73*, 5218–5231.

Gildea, J.J., Herlevsen, M., Harding, M.A., Gulding, K.M., Moskaluk, C.A., Frierson, H.F., and Theodorescu, D. (2004). PTEN can inhibit in vitro organotypic and in vivo orthotopic invasion of human bladder cancer cells even in the absence of its lipid phosphatase activity. Oncogene *23*, 6788–6797.

Gilmore, T.D. (2006). Introduction to NF-kappaB: players, pathways, perspectives. Oncogene *25*, 6680–6684.

Goo, C.K., Lim, H.Y., Ho, Q.S., Too, H.P., Clement, M.V., and Wong, K.P. (2012). PTEN/Akt signaling controls mitochondrial respiratory capacity through 4E-BP1. PLoS ONE *7*, e45806.

Gottlob, K., Majewski, N., Kennedy, S., Kandel, E., Robey, R.B., and Hay, N. (2001). Inhibition of early apoptotic events by Akt/PKB is dependent on the first committed step of glycolysis and mitochondrial hexokinase. Genes Dev. *15*, 1406–1418.

Grassian, A.R., Metallo, C.M., Coloff, J.L., Stephanopoulos, G., and Brugge, J.S. (2011). Erk regulation of pyruvate dehydrogenase flux through PDK4 modulates cell proliferation. Genes Dev. *25*, 1716–1733.

Gu, T., Zhang, Z., Wang, J., Guo, J., Shen, W.H., and Yin, Y. (2011). CREB is a novel nuclear target of PTEN phosphatase. Cancer Res. *71*, 2821–2825.

Gustin, J.A., Maehama, T., Dixon, J.E., and Donner, D.B. (2001). The PTEN tumor suppressor protein inhibits tumor necrosis factor-induced nuclear factor kappa B activity. J. Biol. Chem. *276*, 27740–27744.

Hirai, H., Sootome, H., Nakatsuru, Y., Miyama, K., Taguchi, S., Tsujioka, K., Ueno, Y., Hatch, H., Majumder, P.K., Pan, B.S., and Kotani, H. (2010). MK-2206, an allosteric Akt inhibitor, enhances antitumor efficacy by standard chemotherapeutic agents or molecular targeted drugs in vitro and in vivo. Mol. Cancer Ther. *9*, 1956–1967.

Hlobilkova, A., Guldberg, P., Thullberg, M., Zeuthen, J., Lukas, J., and Bartek, J. (2000). Cell cycle arrest by the PTEN tumor suppressor is target cell specific and may require protein phosphatase activity. Exp. Cell Res. *256*, 571–577.

Houddane, A., Bultot, L., Novellasdemunt, L., Johanns, M., Gueuning, M.A., Vertommen, D., Coulie, P.G., Bartrons, R., Hue, L., and Rider, M.H. (2017). Role of Akt/PKB and PFKFB isoenzymes in the control of glycolysis, cell proliferation and protein synthesis in mitogen-stimulated thymocytes. Cell. Signal. *34*, 23–37.

Jäger, S., Cimermancic, P., Gulbahce, N., Johnson, J.R., McGovern, K.E., Clarke, S.C., Shales, M., Mercenne, G., Pache, L., Li, K., et al. (2011). Global landscape of HIV-human protein complexes. Nature *481*, 365–370.

Jang, M., Kim, S.S., and Lee, J. (2013). Cancer cell metabolism: implications for therapeutic targets. Exp. Mol. Med. *45*, e45.

Kato, M., Li, J., Chuang, J.L., and Chuang, D.T. (2007). Distinct structural mechanisms for inhibition of pyruvate dehydrogenase kinase isoforms by AZD7545, dichloroacetate, and radicicol. Structure *15*, 992–1004.

Kim, J.W., Tchernyshyov, I., Semenza, G.L., and Dang, C.V. (2006). HIF-1-mediated expression of pyruvate dehydrogenase kinase: a metabolic switch required for cellular adaptation to hypoxia. Cell Metab. *3*, 177–185.

Kinoshita, E., Kinoshita-Kikuta, E., and Koike, T. (2009). Separation and detection of large phosphoproteins using Phos-tag SDS-PAGE. Nat. Protoc. *4*, 1513–1521.

Korotchkina, L.G., and Patel, M.S. (2001). Probing the mechanism of inactivation of human pyruvate dehydrogenase by phosphorylation of three sites. J. Biol. Chem. *276*, 5731–5738.

Koul, D. (2008). PTEN signaling pathways in glioblastoma. Cancer Biol. Ther. *7*, 1321–1325.

Koul, D., Yao, Y., Abbruzzese, J.L., Yung, W.K., and Reddy, S.A. (2001). Tumor suppressor MMAC/PTEN inhibits cytokine-induced NFkappaB activation without interfering with the IkappaB degradation pathway. J. Biol. Chem. *276*, 11402–11408.

Lardy, H.A., Johnson, D., and McMURRAY, W.C. (1958). Antibiotics as tools for metabolic studies. I. A survey of toxic antibiotics in respiratory, phosphorylative and glycolytic systems. Arch. Biochem. Biophys. *78*, 587–597.

Lee, J.O., Yang, H., Georgescu, M.M., Di Cristofano, A., Maehama, T., Shi, Y., Dixon, J.E., Pandolfi, P., and Pavletich, N.P. (1999). Crystal structure of the PTEN tumor suppressor: implications for its phosphoinositide phosphatase activity and membrane association. Cell *99*, 323–334.

Lee, H.J., Lee, H.Y., Lee, J.H., Lee, H., Kang, G., Song, J.S., Kang, J., and Kim, J.H. (2014). Prognostic significance of biallelic loss of PTEN in clear cell renal cell carcinoma. J. Urol. *192*, 940–946.

Leslie, N.R., Yang, X., Downes, C.P., and Weijer, C.J. (2007). PtdIns(3,4,5)P(3)-dependent and -independent roles for PTEN in the control of cell migration. Curr. Biol. *17*, 115–125.

Leslie, N.R., Maccario, H., Spinelli, L., and Davidson, L. (2009). The significance of PTEN's protein phosphatase activity. Adv. Enzyme Regul. *49*, 190–196.

Li, D.M., and Sun, H. (1997). TEP1, encoded by a candidate tumor suppressor locus, is a novel protein tyrosine phosphatase regulated by transforming growth factor beta. Cancer Res. *57*, 2124–2129.

Li, J., Yen, C., Liaw, D., Podsypanina, K., Bose, S., Wang, S.I., Puc, J., Miliaresis, C., Rodgers, L., McCombie, R., et al. (1997). PTEN, a putative protein tyrosine phosphatase gene mutated in human brain, breast, and prostate cancer. Science *275*, 1943–1947.

Li, T., Chen, L., Cheng, J., Dai, J., Huang, Y., Zhang, J., Liu, Z., Li, A., Li, N., Wang, H., et al. (2016). SUMOylated NKAP is essential for chromosome alignment by anchoring CENP-E to kinetochores. Nat. Commun. *7*, 12969.

Linn, T.C., Pettit, F.H., and Reed, L.J. (1969). Alpha-keto acid dehydrogenase complexes. X. Regulation of the activity of the pyruvate dehydrogenase complex from beef kidney mitochondria by phosphorylation and dephosphorylation. Proc. Natl. Acad. Sci. U S A *62*, 234–241.

Lunt, S.Y., and Vander Heiden, M.G. (2011). Aerobic glycolysis: meeting the metabolic requirements of cell proliferation. Annu. Rev. Cell Dev. Biol. *27*, 441–464.

Maehama, T., and Dixon, J.E. (1998). The tumor suppressor, PTEN/MMAC1, dephosphorylates the lipid second messenger, phosphatidylinositol 3,4,5-trisphosphate. J. Biol. Chem. *273*, 13375–13378.

Maehama, T., and Dixon, J.E. (1999). PTEN: a tumour suppressor that functions as a phospholipid phosphatase. Trends Cell Biol. *9*, 125–128.

Maehama, T., and Dixon, J.E. (2000). [PTEN tumor suppressor: functions as a lipid phosphatase]. Tanpakushitsu Kakusan Koso *45*, 2405–2414.

Martone, R., Euskirchen, G., Bertone, P., Hartman, S., Royce, T.E., Luscombe, N.M., Rinn, J.L., Nelson, F.K., Miller, P., Gerstein, M., et al. (2003). Distribution of NF-kappaB-binding sites across human chromosome 22. Proc. Natl. Acad. Sci. U S A *100*, 12247–12252.

Mayo, M.W., Madrid, L.V., Westerheide, S.D., Jones, D.R., Yuan, X.J., Baldwin, A.S., Jr., and Whang, Y.E. (2002). PTEN blocks tumor necrosis factor-induced NF-kappa B-dependent transcription by inhibiting the transactivation potential of the p65 subunit. J. Biol. Chem. *277*, 11116–11125.

Millán-Uclés, Á., Zuluaga, S., Marqués, M., Vallejo-Díaz, J., Sanz, L., Cariaga-Martínez, A.E., Real, F.X., and Carrera, A.C. (2016). E-cadherin downregulation sensitizes PTEN-mutant tumors to PI3Kβ silencing. Oncotarget *7*, 84054–84071.

Myers, M.P., Stolarov, J.P., Eng, C., Li, J., Wang, S.I., Wigler, M.H., Parsons, R., and Tonks, N.K. (1997). P-TEN, the tumor suppressor from human chromosome 10q23, is a dual-specificity phosphatase. Proc. Natl. Acad. Sci. U S A *94*, 9052–9057.

Myers, M.P., Pass, I., Batty, I.H., Van der Kaay, J., Stolarov, J.P., Hemmings, B.A., Wigler, M.H., Downes, C.P., and Tonks, N.K. (1998). The lipid phosphatase activity of PTEN is critical for its tumor supressor function. Proc. Natl. Acad. Sci. U S A *95*, 13513–13518.

Neshat, M.S., Mellinghoff, I.K., Tran, C., Stiles, B., Thomas, G., Petersen, R., Frost, P., Gibbons, J.J., Wu, H., and Sawyers, C.L. (2001). Enhanced sensitivity of PTEN-deficient tumors to inhibition of FRAP/mTOR. Proc. Natl. Acad. Sci. U S A *98*, 10314–10319.

Ory, D.S., Neugeboren, B.A., and Mulligan, R.C. (1996). A stable human-derived packaging cell line for production of high titer retrovirus/vesicular stomatitis virus G pseudotypes. Proc. Natl. Acad. Sci. U S A *93*, 11400–11406.

Pajerowski, A.G., Nguyen, C., Aghajanian, H., Shapiro, M.J., and Shapiro, V.S. (2009). NKAP is a transcriptional repressor of notch signaling and is required for T cell development. Immunity *30*, 696–707.

Palmer, G., Horgan, D.J., Tisdale, H., Singer, T.P., and Beinert, H. (1968). Studies on the respiratory chain-linked reduced nicotinamide adenine dinucleotide dehydrogenase. XIV. Location of the sites of inhibition of rotenone, barbiturates, and piericidin by means of electron paramagnetic resonance spectroscopy. J. Biol. Chem. *243*, 844–847.

Patel, M.S., and Roche, T.E. (1990). Molecular biology and biochemistry of pyruvate dehydrogenase complexes. FASEB J. *4*, 3224–3233.

Patel, M.S., Nemeria, N.S., Furey, W., and Jordan, F. (2014). The pyruvate dehydrogenase complexes: structure-based function and regulation. J. Biol. Chem. *289*, 16615–16623.

Pathak, R.R., Grover, A., Malaney, P., Quarni, W., Pandit, A., Allen-Gipson, D., and Davé, V. (2013). Loss of phosphatase and tensin homolog (PTEN) induces leptin-mediated leptin gene expression: feed-forward loop operating in the lung. J. Biol. Chem. *288*, 29821–29835.

Perry, S.W., Norman, J.P., Barbieri, J., Brown, E.B., and Gelbard, H.A. (2011). Mitochondrial membrane potential probes and the proton gradient: a practical usage guide. Biotechniques *50*, 98–115.

Planchon, S.M., Waite, K.A., and Eng, C. (2008). The nuclear affairs of PTEN. J. Cell Sci. *121*, 249–253.

Poburko, D., Santo-Domingo, J., and Demaurex, N. (2011). Dynamic regulation of the mitochondrial proton gradient during cytosolic calcium elevations. J. Biol. Chem. *286*, 11672–11684.

Popov, K.M., Hawes, J.W., and Harris, R.A. (1997). Mitochondrial alpha-ketoacid dehydrogenase kinases: a new family of protein kinases. Adv. Second Messenger Phosphoprotein Res. *31*, 105–111.

Pourmand, G., Ziaee, A.A., Abedi, A.R., Mehrsai, A., Alavi, H.A., Ahmadi, A., and Saadati, H.R. (2007). Role of PTEN gene in progression of prostate cancer. Urol. J. *4*, 95–100.

Rodon, J., Dienstmann, R., Serra, V., and Tabernero, J. (2013). Development of PI3K inhibitors: lessons learned from early clinical trials. Nat. Rev. Clin. Oncol. *10*, 143–153.

Rodríguez-Escudero, I., Oliver, M.D., Andrés-Pons, A., Molina, M., Cid, V.J., and Pulido, R. (2011). A comprehensive functional analysis of PTEN mutations: implications in tumor- and autism-related syndromes. Hum. Mol. Genet. *20*, 4132–4142.

Schneider, C.A., Rasband, W.S., and Eliceiri, K.W. (2012). NIH Image to ImageJ: 25 years of image analysis. Nat Methods *9*, 671–675.

Schulze, A., and Downward, J. (2011). Flicking the Warburg switch-tyrosine phosphorylation of pyruvate dehydrogenase kinase regulates mitochondrial activity in cancer cells. Mol. Cell *44*, 846–848.

Schulze, A., and Harris, A.L. (2012). How cancer metabolism is tuned for proliferation and vulnerable to disruption. Nature *491*, 364–373.

Semenza, G.L. (2008). Tumor metabolism: cancer cells give and take lactate. J. Clin. Invest. *118*, 3835–3837.

Shen, W.H., Balajee, A.S., Wang, J., Wu, H., Eng, C., Pandolfi, P.P., and Yin, Y. (2007). Essential role for nuclear PTEN in maintaining chromosomal integrity. Cell *128*, 157–170.

Shi, Y., Wang, J., Chandarlapaty, S., Cross, J., Thompson, C., Rosen, N., and Jiang, X. (2014). PTEN is a protein tyrosine phosphatase for IRS1. Nat. Struct. Mol. Biol. *21*, 522–527.

Shimizu, S., Eguchi, Y., Kamiike, W., Matsuda, H., and Tsujimoto, Y. (1996a). Bcl-2 expression prevents activation of the ICE protease cascade. Oncogene *12*, 2251–2257.

Shimizu, S., Eguchi, Y., Kamiike, W., Waguri, S., Uchiyama, Y., Matsuda, H., and Tsujimoto, Y. (1996b). Bcl-2 blocks loss of mitochondrial membrane

potential while ICE inhibitors act at a different step during inhibition of death induced by respiratory chain inhibitors. Oncogene *13*, 21–29.

Shimizu, S., Eguchi, Y., Kamiike, W., Funahashi, Y., Mignon, A., Lacronique, V., Matsuda, H., and Tsujimoto, Y. (1998). Bcl-2 prevents apoptotic mitochondrial dysfunction by regulating proton flux. Proc. Natl. Acad. Sci. U S A *95*, 1455–1459.

Shinde, S.R., and Maddika, S. (2016). PTEN modulates EGFR late endocytic trafficking and degradation by dephosphorylating Rab7. Nat. Commun. *7*, 10689.

Soria, J.C., Lee, H.Y., Lee, J.I., Wang, L., Issa, J.P., Kemp, B.L., Liu, D.D., Kurie, J.M., Mao, L., and Khuri, F.R. (2002). Lack of PTEN expression in non-small cell lung cancer could be related to promoter methylation. Clin. Cancer Res. *8*, 1178–1184.

Sos, M.L., Koker, M., Weir, B.A., Heynck, S., Rabinovsky, R., Zander, T., Seeger, J.M., Weiss, J., Fischer, F., Frommolt, P., et al. (2009). PTEN loss contributes to erlotinib resistance in EGFR-mutant lung cancer by activation of Akt and EGFR. Cancer Res. *69*, 3256–3261.

St-Denis, N., Gupta, G.D., Lin, Z.Y., Gonzalez-Badillo, B., Veri, A.O., Knight, J.D.R., Rajendran, D., Couzens, A.L., Currie, K.W., Tkach, J.M., et al. (2016). Phenotypic and interaction profiling of the human phosphatases identifies diverse mitotic regulators. Cell Rep. *17*, 2488–2501.

Stacpoole, P.W. (1989). The pharmacology of dichloroacetate. Metabolism *38*, 1124–1144.

Stambolic, V., Suzuki, A., de la Pompa, J.L., Brothers, G.M., Mirtsos, C., Sasaki, T., Ruland, J., Penninger, J.M., Siderovski, D.P., and Mak, T.W. (1998). Negative regulation of PKB/Akt-dependent cell survival by the tumor suppressor PTEN. Cell *95*, 29–39.

Steck, P.A., Pershouse, M.A., Jasser, S.A., Yung, W.K., Lin, H., Ligon, A.H., Langford, L.A., Baumgard, M.L., Hattier, T., Davis, T., et al. (1997). Identification of a candidate tumour suppressor gene, MMAC1, at chromosome 10q23.3 that is mutated in multiple advanced cancers. Nat. Genet. *15*, 356–362.

Sun, S.Y. (2010). N-acetylcysteine, reactive oxygen species and beyond. Cancer Biol. Ther. *9*, 109–110.

Sun, H., Lesche, R., Li, D.M., Liliental, J., Zhang, H., Gao, J., Gavrilova, N., Mueller, B., Liu, X., and Wu, H. (1999). PTEN modulates cell cycle progression and cell survival by regulating phosphatidylinositol 3,4,5,-trisphosphate and Akt/protein kinase B signaling pathway. Proc. Natl. Acad. Sci. U S A *96*, 6199–6204.

Sun, C., Wang, L., Huang, S., Heynen, G.J., Prahallad, A., Robert, C., Haanen, J., Blank, C., Wesseling, J., Willems, S.M., et al. (2014). Reversible and adaptive resistance to BRAF(V600E) inhibition in melanoma. Nature *508*, 118–122.

Suzuki, K., Bose, P., Leong-Quong, R.Y., Fujita, D.J., and Riabowol, K. (2010). REAP: a two minute cell fractionation method. BMC Res. Notes *3*, 294.

Suzuki, J., Kanemaru, K., Ishii, K., Ohkura, M., Okubo, Y., and Iino, M. (2014). Imaging intraorganellar Ca2+ at subcellular resolution using CEPIA. Nat. Commun. *5*, 4153.

Takahashi, Y., Morales, F.C., Kreimann, E.L., and Georgescu, M.M. (2006). PTEN tumor suppressor associates with NHERF proteins to attenuate PDGF receptor signaling. EMBO J. *25*, 910–920.

Taylor, G.S., and Dixon, J.E. (2003). PTEN and myotubularins: families of phosphoinositide phosphatases. Methods Enzymol. *366*, 43–56.

Teague, W.M., Pettit, F.H., Yeaman, S.J., and Reed, L.J. (1979). Function of phosphorylation sites on pyruvate dehydrogenase. Biochem. Biophys. Res. Commun. *87*, 244–252.

Thapa, P., Chen, M.W., McWilliams, D.C., Belmonte, P., Constans, M., Sant'Angelo, D.B., and Shapiro, V.S. (2016). NKAP regulates invariant NKT cell proliferation and differentiation into ROR-γt-expressing NKT17 cells. J. Immunol. *196*, 4987–4998.

Tibarewal, P., Zilidis, G., Spinelli, L., Schurch, N., Maccario, H., Gray, A., Perera, N.M., Davidson, L., Barton, G.J., and Leslie, N.R. (2012). PTEN protein phosphatase activity correlates with control of gene expression and invasion, a tumor-suppressing phenotype, but not with AKT activity. Sci. Signal. *5*, ra18.

Tristan, C., Shahani, N., Sedlak, T.W., and Sawa, A. (2011). The diverse functions of GAPDH: views from different subcellular compartments. Cell. Signal. *23*, 317–323.

Tsujimoto, Y. (1998). Role of Bcl-2 family proteins in apoptosis: apoptosomes or mitochondria? Genes Cells *3*, 697–707.

Tsunoda, T., and Takagi, T. (1999). Estimating transcription factor bindability on DNA. Bioinformatics *15*, 622–630.

Vander Heiden, M.G., Cantley, L.C., and Thompson, C.B. (2009). Understanding the Warburg effect: the metabolic requirements of cell proliferation. Science *324*, 1029–1033.

Wan, F., and Lenardo, M.J. (2009). Specification of DNA binding activity of NF-kappaB proteins. Cold Spring Harb. Perspect. Biol. *1*, a000067.

Wang, L., Xiong, H., Wu, F., Zhang, Y., Wang, J., Zhao, L., Guo, X., Chang, L.J., Zhang, Y., You, M.J., et al. (2014). Hexokinase 2-mediated Warburg effect is required for PTEN- and p53-deficiency-driven prostate cancer growth. Cell Rep. *8*, 1461–1474.

Warburg, O. (1956). On the origin of cancer cells. Science *123*, 309–314.

Whitehouse, S., Cooper, R.H., and Randle, P.J. (1974). Mechanism of activation of pyruvate dehydrogenase by dichloroacetate and other halogenated carboxylic acids. Biochem. J. *141*, 761–774.

Wittenberg, A.D., Azar, S., Klochendler, A., Stolovich-Rain, M., Avraham, S., Birnbaum, L., Binder Gallimidi, A., Katz, M., Dor, Y., and Meyuhas, O. (2016). Phosphorylated ribosomal protein S6 is required for Akt-driven hyperplasia and malignant transformation, but not for hypertrophy, aneuploidy and hyperfunction of pancreatic β-cells. PLoS ONE *11*, e0149995.

Wozniak, D.J., Kajdacsy-Balla, A., Macias, V., Ball-Kell, S., Zenner, M.L., Bie, W., and Tyner, A.L. (2017). PTEN is a protein phosphatase that targets active PTK6 and inhibits PTK6 oncogenic signaling in prostate cancer. Nat. Commun. *8*, 1508.

Wykoff, C.C., Beasley, N.J., Watson, P.H., Turner, K.J., Pastorek, J., Sibtain, A., Wilson, G.D., Turley, H., Talks, K.L., Maxwell, P.H., et al. (2000). Hypoxia-inducible expression of tumor-associated carbonic anhydrases. Cancer Res. *60*, 7075–7083.

You, D., Xin, J., Volk, A., Wei, W., Schmidt, R., Scurti, G., Nand, S., Breuer, E.K., Kuo, P.C., Breslin, P., et al. (2015). FAK mediates a compensatory survival signal parallel to PI3K-AKT in PTEN-null T-ALL cells. Cell Rep. *10*, 2055–2068.

Zhao, Y., Butler, E.B., and Tan, M. (2013). Targeting cellular metabolism to improve cancer therapeutics. Cell Death Dis. *4*, e532.

STAR★METHODS

KEY RESOURCES TABLE

REAGENT or RESOURCE	SOURCE	IDENTIFIER
Antibodies		
Rabbit anti-PTEN	Cell Signaling Technology	Cat# 9188; RRID: AB_2253290
Mouse anti-AKT (pan)	Cell Signaling Technology	Cat# 2920; RRID: AB_1147620
Rabbit anti-p-AKT (S473)	Cell Signaling Technology	Cat# 4060; RRID: AB_2315049
Mouse anti-β Actin	Sigma-Aldrich	Cat# A2228; RRID: AB_476697
Rabbit anti-PDHK1	Cell Signaling Technology	Cat# 3820; RRID: AB_1904078
Mouse polyclonal anti-PDK2	Abcam	Cat# ab172065
Rabbit polyclonal anti-PDK3	Abcam	Cat# ab154549
Goat polyclonal anti-PDK4	Santa Cruz Biotechnology	Cat# sc-14495 *(discontinued)*
Rabbit polyclonal anti-p-PDHE1A (S293)	Millipore	Cat# ABS204; RRID: AB_11205754
Mouse anti-cleaved PARP	Cell Signaling Technology	Cat# 9546; RRID: AB_2160593
Mouse anti-GAPDH	Santa Cruz Biotechnology	Cat# sc-365062; RRID: AB_10847862
Rabbit polyclonal anti-p-S6 (S240/S244)	Cell Signaling Technology	Cat# 2215; RRID: AB_331682
Rabbit anti-NFκB p65	Cell Signaling Technology	Cat# 8242; RRID: AB_10859369
Rabbit anti-p- NFκB p65 (S536)	Cell Signaling Technology	Cat# 3033; RRID: AB_331284
Rabbit anti-Lamin B1	Cell Signaling Technology	Cat# 12586; RRID: AB_2650517
Rabbit polyclonal anti-HSP90	Cell Signaling Technology	Cat# 4874; RRID: AB_2121214
Rabbit polyclonal anti-HSP60	Cell Signaling Technology	Cat# 4870; RRID: AB_2295614
Rabbit polyclonal anti-H3	Cell Signaling Technology	Cat# 9715; RRID: AB_331563
Rabbit polyclonal anti-NKAP	Abcam	Cat# ab121121; RRID: AB_11139756
Mouse anti-NKAP (K85-80-5)	Burgute et al., 2014	N/A
Rabbit polyclonal anti-V5	Sigma-Aldrich	Cat# V8137; RRID: AB_261889
Mouse anti-FLAG M2	Sigma-Aldrich	Cat# F1804; RRID: AB_262044
Mouse anti-GST	Cell Signaling Technology	Cat# 2624; RRID: AB_2189875
Rabbit anti-HA	Cell Signaling Technology	Cat# 3724; RRID: AB_1549585
Mouse anti-Cytochrome *c*	Abcam	Cat# ab13575; RRID: AB_300470
Rabbit anti-VDAC	Cell Signaling Technology	Cat# 4661; RRID: AB_10557420
Rabbit polyclonal anti-Caspase 9	Cell Signaling Technology	Cat# 9502; RRID: AB_2068621
Rabbit polyclonal anti-Caspase 7	Cell Signaling Technology	Cat# 9492; RRID: AB_2228313
Mouse monoclonal anti-Caspase 3	Cell Signaling Technology	Cat# 9668; RRID: AB_206987
Rabbit polyclonal anti-cleaved Caspase 9	Cell Signaling Technology	Cat# 9505; RRID: AB_2290727
Rabbit polyclonal anti-cleaved Caspase 7	Cell Signaling Technology	Cat# 9491; RRID: AB_2068144
Rabbit polyclonal anti-cleaved Caspase 3	Cell Signaling Technology	Cat# 9661; RRID: AB_2341188
Rabbit anti-BCL-xL	Cell Signaling Technology	Cat# 2764; RRID: AB_2228008
Rabbit anti-BCL2	Cell Signaling Technology	Cat# 4223; RRID: AB_1903909
Rabbit polyclonal anti-p-GSK-3α/β (S21/9)	Cell Signaling Technology	Cat# 9331; RRID: AB_329830
Rabbit anti-HK2	Cell Signaling Technology	Cat# 2867; RRID: AB_2232946
Rabbit polyclonal anti-HIF-1α	Cell Signaling Technology	Cat# 3716
Rabbit anti-CA9	Cell Signaling Technology	Cat# 5649; RRID: AB_10706355
Bacterial and Virus Strains		
PTEN adenovirus (human)	Applied Biological Materials	Cat# 000028A
PDK1-HA adenovirus (human)	Applied Biological Materials	Cat# 119140A

(*Continued on next page*)

Continued

REAGENT or RESOURCE	SOURCE	IDENTIFIER
Biological Samples		
Brain tumor tissue microarray	US Biomax	Cat# GL1921
Prostate adenocarcinoma tissue microarray	US Biomax	Cat# PR803a
Lung Carcinoma tissue microarray	US Biomax	Cat# LC801
Chemicals, Peptides, and Recombinant Proteins		
BKM120 (PI3K inhibitor)	Selleckchem	Cat# S2247
GDC-0941 (PI3K inhibitor)	Selleckchem	Cat# S1065
MK-2206 (AKT inhibitor)	Selleckchem	Cat# S1078
DCA (PDHK inhibitor)	Sigma-Aldrich	Cat# 347795
PBS-1086 (NF-κB inhibitor)	Blakely et al., 2015	N/A
Bay 11-7085 (NF-κB inhibitor)	Selleckchem	Cat# S7352
Cisplatin	Selleckchem	Cat# S1166
Docetaxel	Selleckchem	Cat# S1148
NAC	Sigma-Aldrich	Cat# A7250
H2DCFDA	Thermo Fisher Scientific	Cat# D399
Rotenone (ETC complex I inhibitor)	Abcam	Cat# ab143145
Oligomycin (ATP synthase inhibitor)	Abcam	Cat# ab141829
2-DG	Sigma-Aldrich	Cat# D8375
Human TNF-α	Peprotech	Cat# 300-01A
Human NKAP-p-S9 peptide (SGSR-p-SPDREA)	Elim Biopharmaceuticals	This paper
Human NKAP-pS149 peptide (VWGL-p-SPKNPE)	Elim Biopharmaceuticals	This paper
Human Rab7-p-S72 peptide (ERFQ-p-SLGVAF)	Elim Biopharmaceuticals	This paper
Critical Commercial Assays		
DC Protein Assay	Bio-Rad	Cat# 500-0116
Trans-Blot Turbo RTA Midi Nitrocellulose Transfer kit	Bio-Rad	Cat# 170-4271
RNeasy kit	QIAGEN	Cat# 74106
CellTiter-Glo Cell Viability Assay	Promega	Cat# G7573
L-lactate Assay	Cayman	Cat# 700510
SimpleChIP Enzymatic Chromatin IP Kit	Cell Signalling Technology	Cat# 9003
EpiTect ChIP qPCR Primer Assay for human PDK1, NM_002610.3 (-)01Kb	Qiagen	Cat# GPH1007880 (-)01A
TaqMan Gene Expression Assay (FAM) for human PDK1, Hs01561850_m1	Thermo Fisher Scientific	Cat# 4331182
TaqMan Gene Expression Assay (FAM) for human GAPDH, Hs99999905_m1	Thermo Fisher Scientific	Cat# 4331182
Bright-Glo Luciferase Assay	Promega	Cat# E2610
Malachite Green Assay	Echelon	Cat# K1500
Cytochrome c Release Assay	Abcam	Cat# ab65311
Deposited Data		
Raw and analyzed microarray data	This paper	GEO: GSE121217
Raw and analyzed phospho-proteomics data	This paper	PRIDE: PXD014707
Experimental Models: Cell Lines		
Human lung adenocarcinoma H1650	Laboratory of William Pao	N/A
Human lung Adenocarcinoma H1975	Laboratory of William Pao	N/A
Human lung Adenocarcinoma HCC827	Laboratory of William Pao	N/A
Human prostate Adenocarcinoma PC3	ATCC	Cat# CRL-1435
Human renal clear cell carcinoma 786-O	Laboratory of M. Celeste Simon	N/A
Human lung squamous carcinoma H520	ATCC	Cat# HTB-182

(*Continued on next page*)

Continued

REAGENT or RESOURCE	SOURCE	IDENTIFIER
Human skin cutaneous melanoma A2058	ATCC	Cat# CRL-11147
Human glioblastoma multiforme U87MG	ATCC	Cat# HTB-14
Human embryonic kidney cells 293T	ATCC	Cat# CRL-3216
Human bronchial epithelial cells BEAS2B	ATCC	Cat# CRL-9609
Experimental Models: Organisms/Strains		
Mouse: C.B-*Igh-1*^{b}/IcrTac-*Prkdc*^{scid}	Taconic Biosciences	Cat# CB17SC-F
Oligonucleotides		
PTEN Mission shRNA (3'-UTR): CCGGCCACAAATGAAGGGATATAAACTCGAGTTTATATC CCTTCATTTGTGGTTTTTG	Sigma-Aldrich	Cat# TRCN0000230370
PDHK1 Mission shRNA (CDS) #1: CCGGGCTCTGTCAACAGACTCAATACTCGAGTATTGAG TCTGTTGACAGAGCTTTTT	Sigma-Aldrich	Cat# TRCN0000006261
PDHK1 Mission shRNA (CDS) #2: CCGGCCAGGGTGTGATTGAATACAACTCGAGTTGTATT CAATCACACCCTGGTTTTT	Sigma-Aldrich	Cat# TRCN0000006263
PDHK1 Mission shRNA (3'-UTR): CCGGGAAGTAGAAGTCTACCATATTCTCGAGAATATGG TAGACTTCTACTTCTTTTTTG	Sigma-Aldrich	Cat# TRCN0000196728
RELA Mission shRNA (3'-UTR): CCGGGCCTTAATAGTAGGGTAAGTTCTCGAGAACTTAC CCTACTATTAAGGCTTTTT	Sigma-Aldrich	Cat# TRCN0000014683
NKAP Mission shRNA (3'-UTR): CCGGCTGATTGTCCAGAAGACATTTCTCGAGAAATGTC TTCTGGACAATCAGTTTTTG	Sigma-Aldrich	Cat# TRCN0000145605
NKAP Mission shRNA (CDS): CCGGGCTGAAGAACCATCAGATTTACTCGAGTAAATCT GATGGTTCTTCAGCTTTTTG	Sigma-Aldrich	Cat# TRCN0000145475
ON-TARGETplus Non-targeting Pool siRNA	Dharmacon	Cat# D-001810-10
SMARTpool: ON-TARGETplus PDK1 siRNA	Dharmacon	Cat# L-005019-00-0005
SMARTpool: ON-TARGETplus HIF1A siRNA	Dharmacon	Cat# L-004018-00-0005
Recombinant DNA		
pLKO.1-puro Non-Target shRNA	Sigma-Aldrich	Cat# SHC016
pBABE-Puro-EV	Addgene	Cat# 1764
pBABE-GFP	Addgene	Cat# 10668
pBABE-PTEN	Addgene	Cat# 10785
pBABE-PTEN^{C124S}	Addgene	Cat# 10931
pBABE-PTEN^{G129E}	Addgene	Cat# 10771
pBABE-PTEN^{Y138L}	This paper	N/A
pCDH-Puro-EV	This paper	N/A
pCDH-puro-Bcl2	Addgene	Cat# 46971
pCDH-puro-Bcl-xL	Addgene	Cat# 46972
pCW22-TRE-Blast-EV	This paper	N/A
pCW22-TRE-blast-NKAP-HA-FLAG	This paper	N/A
pCW22-TRE-blast-NKAP^{S9AS149A}-HA-FLAG	This paper	N/A
pLV-EF1a-IRES-Hygro	Addgene	Cat# 85134
pLV-EF1a-IRES-Hygro-PDHK1	This paper	N/A
pCMV-2xFLAG- PTEN	Addgene	Cat# 28298
pLX304-NKAP-V5	Dharmacon	Cat# OHS6085-213576668
pEBG-GST-NHERF2	Addgene	Cat# 28292
pET-30 b-PTEN-6xHis	Addgene	Cat# 20741

(*Continued on next page*)

Continued		
REAGENT or RESOURCE	SOURCE	IDENTIFIER
pET-30 b-PTEN^{Y138L}-6xHis	This paper	N/A
pGreenFire1-NF-kB (EF1α-Puro)	System Biosciences	Cat# TR012PA-P
Plasmid: LightSwitch PDK1 Promoter Reporter	SwitchGear Genomics	Cat# S721832
Software and Algorithms		
ImageJ	Schneider et al., 2012	https://imagej.nih.gov/ij/
GraphPad Prism 6	GraphPad	RRID:SCR_002798

LEAD CONTACT AND MATERIALS AVAILABILITY

Further information and requests for resources and reagents should be directed to and will be fulfilled by the Lead Contact, Trever Bivona (trever.bivona@ucsf.edu). This study did not generate new unique reagents.

EXPERIMENTAL MODEL AND SUBJECT DETAILS

Animals

Female, 4-5 weeks old NOD/SCID mice were obtained from Taconic Biosciences. All animal studies followed the NIH Guidelines and AAALAC International standards set for the ethical use and care of laboratory animals, NRC 2011 and were conducted under a UCSF IACUC approved animal protocol (AN107889).

Cell cultures

All cell lines were grown in RPMI-1640 or DMEM (GE Healthcare) supplemented with 10% fetal bovine serum (Sigma-Aldrich) and 100 U/ml penicillin G and 100 μg/ml streptomycin (GE Healthcare) at 37°C under 5% CO_2. For hypoxia experiments, 24 hours after cell seeding cells were incubated at 37°C for indicated times in a sealed hypoxia chamber filled with 1% O_2, 4% CO_2 and 95% N_2.

METHOD DETAILS

Transfection and viral infection

293T cells were transfected with various plasmids using *Trans*IT-LT1 transfection reagent (Mirus Bio) according to manufacturer's instructions. Briefly, plasmid DNA diluted in serum-free OptiMEM medium was mixed with *Trans*IT-LT1 transfection reagent at 1:3 ratio. After incubating the DNA-TransIT-LT1 mixture at room temperature for 15 min, the complexes were added to cells to allow the transfection of plasmid DNA.

293T cells were transfected with various lentiviral constructs and packaging plasmids using calcium phosphate or *Trans*IT-LT1 (Mirus Bio) transfection reagent according to manufacturer's instructions. Three days post-transfection lentiviral supernatant supplemented with 6 μg/ml of polybrene was used to infect the indicated cell lines. 48 hours post-infection cells were replated with antibiotic containing media and selection was continued for an additional 2-7 days. Experiments were performed with the cells that survived antibiotic selection (stable cell lines).

293-GPG viral packaging cells (Ory et al., 1996) were transfected with various p-BABE-Puro retroviral constructs using Lipofectamine-2000 (Invitrogen) according to manufacturer's instructions. Three days post-transfection retroviral supernatant supplemented with 6 μg/ml polybrene was used to transduce various cancer and normal cell lines. 48 hours post-infection cells were replated with Puromycin (1-2 μg/ml) containing media and selection was continued for an additional 4 days. Cells that survived puromycin selection (stable cell lines) were used in subsequent experiments.

High titer pre-made adenovirus expressing PTEN (Applied Biological Materials) was used to transduce the indicated PTEN-deficient cell lines to transiently overexpress PTEN. High titer pre-made adenovirus expressing PDHK1-HA (Applied Biological Materials) was used to infect PTEN-deficient H1650 cells with stable PDHK1 knockdown for transient overexpression of shRNA-resistant PDHK1-HA.

Cell viability and growth assays

Cells were plated at a density of 5,000 cells per well in 96-well plates 24 hours before drug treatment. The number of viable cells was determined 72 hours after the initiation of drug treatment using CellTiter-Glo luminescent cell viability reagent according to the manufacturer's instructions (Promega). Each assay consisted of five to eight replicate wells. Data are expressed as percentage of the cell viability of control cells. Data were graphically displayed using GraphPad Prism version 6.0 for Mac (GraphPad Software).

When cell viability was measured in an ATP independent assay, cells (200,000) were plated per well in 6-well plates 24 hours prior to drug treatment. 72 hours post-drug treatment cells were fixed with 4% paraformaldehyde. 0.05% Crystal violet was used to stain the viable cells and imaged using an ImageQuant LAS 4000 instrument (GE Healthcare). The crystal violet staining based viability assay

measures the anchorage-dependent growth of adherent cells and hence whether the targeted cells are dying or not could be determined from this assay. To quantify the number of viable cells, stained cells were solubilized in 1% SDS and absorbance was measured at 590 nm in a plate reader (SpectraMax M5, Molecular devices).

For the determination of rescue score, cells were treated with a dose-response of DCA and stained with crystal violet 72 hours after treatment. For each cell line, the degree of cell viability at the highest concentration of DCA (20 mM) was normalized to the vehicle control for each genetic background (cells expressing GFP or $PTEN^{WT}$ or $PTEN^{Mutant}$). This normalized cell viability value was then used to calculate the rescue score as: normalized viability in the PTEN-reconstitution condition/ normalized viability in the PTEN-deficient, GFP, condition. A rescue score > 1 indicates the degree of rescue from lethality upon PDHK1 inhibition.

Intracellular ATP and ROS measurement

Intracellular levels of ATP were measured by using CellTiter-Glo luminescent assay (Promega), according to manufacturer's instructions. For each cell line, 5,000 cells were plated per well of 96 well plates. After 24 hours, cells were treated with 100 nM of rotenone for 2 hours or with 100 μM of oligomycin for 1 hour at 37°C to quickly achieve the maximal inhibition of complex I or V, respectively, while not to induce cell death during the experimental period. Relative ATP levels (% of untreated) were calculated.

For measurement of intracellular ROS levels, 20,000 cells of A2058 or PC3 cells or 15,000 cells of H1650 cells were plated per well of 96 well plates. After 24 hours, cells were washed once with serum free RPMI media without phenol red and incubated with 2.5 μM of 2′,7′-dichlorodihydrofluorescein diacetate (H2DCFDA) solution in serum free RPMI media without phenol red for 1 hour at 37°C. The H2DCFDA solution was removed and cells were treated with 40 or 50 mM DCA with or without 1 mM NAC or with only 1 mM NAC in serum free RPMI media without phenol red. After 24 hours of indicated treatment, the 2′,7′-dichlorofluorescein (DCF) fluorescence was measured with a plate reader (SpectraMax M5, Molecular devices) at Ex/Em: 485 nm/538 nm. Relative ROS levels (% of untreated) were calculated.

L-lactate measurement

Extracellular L-lactate was measured using a lactate assay kit (Cayman) following manufacturer's instructions. Briefly, cells were plated at equal numbers in at least 8 micro wells per condition and cultured with the same volume of media. The assay employs the feature of NAD^+ reduction to NADH which occurs concomitantly with the oxidation of lactate to pyruvate. NADH reacts with the fluorescent substrate to produce high fluorescence at Ex/Em: 540 nm/590 nm. The greater the signal the higher is the lactate concentration in the culture media. For glucose conditioned media, RPMI or DMEM without glucose was used (GIBCO) and 2DG (2-deoxyglucose) was supplemented at 10 mM final concentration.

Protein blot analysis

Cells (200,000) were seeded per well in 6-well plates 24 h before drug treatment, and whole-cell lysates were prepared using RIPA buffer (10 mM Tris-HCl (pH 8.0), 1 mM EDTA, 0.1% sodium deoxycholate, 0.1% SDS, 140 mM NaCl) supplemented with protease inhibitor and phosphatase inhibitor (Pierce) and clarified by sonication and centrifugation. Nuclear and cytosolic fractionation was performed as described before (Suzuki et al., 2010). Mitochondrial and cytosolic fractionation was performed using Cytochrome *c* release assay reagents (Abcam). Equal amounts of protein were separated by 4%–15% gradient SDS-PAGE and were transferred onto nitrocellulose membranes (Bio-Rad) for protein blot analysis. Membranes were incubated with primary antibody overnight, washed and incubated with secondary antibody. Membranes were developed using either a fluorescence system (Li-Cor) or a chemiluminescent reagent; images were captured, and bands were quantified using an ImageQuant LAS 4000 instrument (GE Healthcare).

Gene expression profiling

Three biological replicate retroviral infections of H1650 cells were performed with pBABE-PTEN or pBABE-GFP as described above, followed by selection in 2 μg/ml puromycin for 2 days. Stable PTEN expression was confirmed by immunoblot analysis 5 days post-infection. Total RNA was isolated for each replicate using the RNeasy kit (QIAGEN) according to manufacturer's instructions. After quality control validation, 2 μg of total RNA was processed for hybridization and image quantification of U133A 2.0 gene expression arrays (Affymetrix).

Real time qRT-PCR

PDHK1 gene expression changes observed by microarray analysis were validated by real-time qRT-PCR in paired cell lines engineered to stably lack or express PTEN. PDHK1 gene expression regulation by different phosphatase activities of PTEN was also measured by real-time qRT-PCR in PTEN-deficient cell lines stably expressing $PTEN^{WT}$, $PTEN^{G129E}$, $PTEN^{Y138L}$ or GFP. Briefly, for real time qRT-PCR analysis total RNA was extracted from cultured cells using the RNeasy kit (QIAGEN). cDNA was synthesized with SuperScript III reverse transcriptase using random hexamer primers (Invitrogen) and Real time qRT-PCR was performed on the QuantStudio 12K Flex real-time qPCR system using Taqman probes (human PDK1: Assay ID, Hs01561850_m1, Applied Biosystems). GAPDH expression was used as an internal control to normalize input cDNA (human GAPDH: Assay ID, Hs99999905_m1, Applied Biosystems). Ratios of the expression level of each gene to that of the reference gene were then calculated.

Chromatin immunoprecipitation (ChIP) assays

ChIP assays were performed using the chromatin IP kit (Cell Signaling Technology) following manufacturer's instructions. Briefly, $4x10^7$ cells were treated with formaldehyde to crosslink proteins to DNA and nuclear/cytosolic fractionation was performed. Nuclear lysates were sonicated using the Covaris S2 sonicator and an aliquot of DNA was purified to check for sonication efficiency (fragments of ~500bp). Anti-p65, anti-IgG and anti-H3 (positive control) antibodies were used to pull down the indicated protein-bound chromatin. Washing, elution and reverse crosslink followed by DNA purification concluded the sample preparation. Quantification of NF-κB (or RELA) enrichment was done using real-time qPCR with primers designed to amplify a 118 bp region spanning nucleotide position 173420380 in the PDHK1 promoter (EpiTect ChIP qPCR Primer Assay for human PDK1, NM002610.3 (-)01Kb, QIAGEN). Assay position: Chromosome 2, 173420380, TSS position: Chromosome 2, 173420779, Assay tile: (-) 01Kb). A standard curve was generated to examine the efficiency of amplification by plotting Ct (threshold cycle) versus DNA quantity (Log_{10} scale). The fold enrichment was calculated using the following two formulas: Formula 1: $Y = M(Log_{10}X) + B$ (X = DNA quantity, Y = Ct, M = slope of the curve, B = Ct value where X = 1). Formula 2: Fold enrichment = (ChIP DNA Quantity)/ (IgG DNA Quantity).

Luciferase reporter assays

pGreenFire1-NF-κB (EF1α-Puro) lentiviral plasmid containing four NF-κB transcription factor response elements fused in tandem upstream of a luciferase gene under a minimal CMV promoter was transfected into PTEN-deficient cancer cells stably expressing either $PTEN^{WT}$ or $PTEN^{G129E}$ or $PTEN^{Y138L}$ or GFP to measure the effects of PTEN's protein and / or lipid phosphatase activities on the transcriptional activity of NF-κB. pGreenFire1-NF-κB (EF1α-Puro) reporter plasmid was also transfected into PTEN-deficient cells stably expressing $NKAP^{WT}$ or $NKAP^{s9AS149A}$ or with stable NKAP knockdown to study the effects of NKAP phosphorylation on NF-κB activity. PDK1 promoter reporter plasmid containing the PDHK1 promoter fused to luciferase was transfected into PTEN-deficient cancer cell lines with stable NKAP knockdown to measure the effects of NKAP downregulation on PDHK1 promoter activation. Luciferase activity was measured 24 hours after transfection. Cells were washed with phenol-red minus DMEM media once and luciferase detection reagent was added (Bright-Glo, Promega, Cat# E2610) at 100 μL per well and luminescence was measured after 5 min of incubation at RT in a plate reader (SpectraMax M5, Molecular devices).

In vitro phosphatase assays

5-14 amino acid (SGSRpSPDREA) p-S9-NKAP or 145-154 amino acid (VWGLpSPKNPE) p-S149-NKAP or 68-77 amino acid (ERFQpSLGVAF) p-S72-Rab7 peptide (used as a +ve control) was incubated without or with bacterially expressed and purified (as described before (Taylor and Dixon, 2003)) $PTEN^{WT}$ or mutant Y138L PTEN enzyme in reaction buffer (25mM HEPES, pH 7.5, 10 mM MgCl2, 10 mM DTT) at 37°C for 90 min. Following incubation, the released phosphate from each phospho-peptide ± $PTEN^{WT}$ or mutant Y138L PTEN enzyme was detected using Malachite Green Assay Kit (Echelon) by measuring the absorbance at 620 nm in a plate reader (SpectraMax M5, Molecular devices).

Phos-tag assays

Phos-tag PAGE analysis was carried out to detect phosphorylated-NKAP and its de-phosphorylated species according to manufacturer's instructions (Wako Chemicals, Japan). Briefly, PTEN-deficient cancer cells stably expressing either $PTEN^{WT}$ or $PTEN^{G129E}$ or $PTEN^{Y138L}$ or GFP were lysed and subjected to Zinc-based polyacrylamide gel electrophoresis. After electrophoresis, Phos-tag acrylamide gels were washed with gentle shaking in transfer buffer containing 10 mM EDTA for 30 min and then incubated in transfer buffer without EDTA for 15 min. Proteins were then transferred to nitrocellulose membrane for further analysis by standard immunoblotting protocol using specific antibodies.

Immunoprecipitation

For immunoprecipitation assays, 48 hours post-transfection of different plasmids in 293T cells, the cells were resuspended in lysis buffer (200 mM NaCl, 0.5 mM EDTA, 0.5% NP40, 50 mM Tris.Cl, pH 7.5) containing 250 U Benzonase (SIGMA)/ 5 mL and protease inhibitors and lysed by a rapid freeze-thaw cycle (10 min on dry ice followed by 1 min at 37°C). The whole-cell extracts (WCE) obtained by centrifugation were incubated overnight with M2 agarose-FLAG beads (SIGMA) at 4°C. The immunocomplexes were washed once with wash buffer I (50 mM Tris (pH 7.4, 150 mM NaCl, 0.05% NP40), three more times with wash buffer II (50 mM Tris (pH 7.4, 150 mM NaCl), eluted from the beads with elution buffer (150 ng/ μl FLAG peptide in wash buffer II) and applied to SDS-PAGE.

Time-lapse imaging

A2058 empty vector or stable PTEN expressing cells were plated at 50,000 cells per well in a 24 well plate on Day zero. Cells were transfected with SypHer-dmito construct (Suzuki et al., 2014) using Xfect (Clontech) on Day 1 and treated without or with 50 mM DCA on Day 2 for 2 hr at 37°C in normal culture medium. Immediately before image acquisition by time-lapse microscopy, media was replaced with physiological salt solution (PSS) containing 150 mM NaCl, 4 mM KCl, 2 mM CaCl2, 1 mM MgCl2, 5.6 mM glucose and 25 mM HEPES (pH 7.4) ± 50 mM DCA at 37°C. Images were acquired with CMOS image sensor, ORCA-Flash 4.0 (Hamamatsu, Japan), equipped with 418-442 nm and 450-490 nm excitation filters, and 510-540 nm emission filter. SypHer-dmito fluorescence (F470/F430) ratio was calculated for each cell after subtracting background signal. All images were analyzed with ImageJ

software (Schneider et al., 2012). For each cell type, cells with F470/F430 ratio values greater than two s.d. from the mean value were excluded.

Immunohistochemistry

For immunohistochemistry, 5-15 μm thick formalin-fixed paraffin embedded (FFPE) human tissue sections were purchased from US Biomax (Glioblastoma multiforme, Prostate adenocarcinoma and Lung Carcinoma) and stained with PTEN or PDHK1 antibodies following manufacturer's instructions. Stained slides were digitized using the Aperio ScanScope slide scanner (Aperio Technologies) with a 40x objective. Scanned images from the immunohistochemistry staining were used to score expression of PTEN or PDHK1 in paired samples (scoring expression on a scale of 1 to 3, with 1 indicating 'low', 2 'intermediate', and 3 'high' expression of each protein). Bars indicate 50 μm and arrows indicate representative tumor cells scored for PTEN and PDHK1 expression.

Phospho-proteomics study

GFP or $PTEN^{WT}$ or $PTEN^{G129E}$ or $PTEN^{Y138L}$ was stably introduced in two different PTEN-deficient cancer cell lines H1650 and A2058 with different genetic and histologic backgrounds. Cells were lysed in a buffer containing 8M urea, 100 mM Tris.Cl pH 8.0, 150 mM NaCl, and protease inhibitors (EDTA free cOmplete cocktail tablet, Roche). Lysates were reduced with 4 mM TCEP for 30 minutes at room temperature and alkylated with 10 mM iodoacetamide for 30 minutes at room temperature in the dark. Samples were diluted 1:4 in 100 mM Tris pH 8.0 to reduce urea concentration to 2M and digested with trypsin (1:100 enzyme: substrate ratio) overnight at 37°C. Peptides were desalted with Sep-Pak reversed phase C18 solid phase extraction (Waters) according the manufacturer's instructions and phosphopeptides were purified using an immobilized metal affinity chromatography approach. Purified phosphopeptides were analyzed in an LTQ Orbitrap Elite mass spectrometry system (Thermo Scientific) equipped with a Proxeon Easy nLC 1000 ultra high-pressure liquid chromatography and auto sampler system. Samples were injected onto a C18 column (25 cm x 75 um I.D. packed with ReproSil Pur C18 AQ 1.9 um particles) in 0.1% formic acid and then subjected to a 4-hour gradient from 0.1% formic acid to 30% ACN/0.1% formic acid. The mass spectrometer collected data in a data-dependent fashion, collecting one full scan in the Orbitrap at 120,000x resolution followed by 20 collision-induced dissociation MS/MS scans in the dual linear ion trap for the 20 most intense peaks from the full scan. Dynamic exclusion was enabled for 30 s with a repeat count of 1. Charge state screening was employed to reject analysis of singly charged species or species for which a charge could not be assigned.

Colony formation assays

50,000 cells were seeded in 0.35% Noble-agar overlaying 0.6% Noble agar base in 60 mm dishes (Falcon). Cells were grown for 21-28 days and media was changed after every 4 days. Colonies were visualized after staining with 0.005% crystal violet, imaged and quantified.

Animal studies

A2058-GFP and A2058-PTEN tumor xenografts were generated by injection of $2x10^6$ cells/ tumor mixed with matrigel in NOD/SCID mice. Stable PTEN re-expression in PTEN-deficient A2058 cells was confirmed by immunoblotting before *in vivo* transplantation. Tumors were allowed to grow until they reached a minimum volume of 200 mm^3 at Day 17 when both group of animals (with GFP and PTEN expressing tumors) received treatment with DCA (750 mg/ L) in drinking water. Tumor growth was assessed at the indicated time-points by caliper measurements over 31 days post *in vivo* transplantation and data shown represent the endpoint of the study. A minimum of 6 tumors per treatment group was assessed for the duration of the study.

QUANTIFICATION AND STATISTICAL ANALYSIS

Statistical analyses

Statistical differences between two experimental groups were calculated using the unpaired two-tailed Student's t test. Statistical differences between multiple experimental groups were calculated using the multiple comparisons one-way ANOVA test. Statistical differences of tumor volumes were calculated using the two-way ANOVA test. A significance level of $p < 0.05$ or less was used throughout the study. Replicate information is reported in the figure legends.

TCGA data analysis

Data preparation: TCGA pan-cancer gene expression by RNaseq using the Illumina HiSeq technology was downloaded (https://toil.xenahubs.net/download/tcga_RSEM_Hugo_norm_count.gz). Data from all TCGA cohorts (N = 10535) were combined to produce this dataset. Values are Log_2 (x+1) transformed RSEM values.

TCGA pan-cancer gene-level copy number variation (CNV) estimated using the GISTIC2 threshold method was downloaded. Data from all TCGA cohorts (N = 10845) were combined to produce this dataset. GISTIC2 further thresholded the estimated values to −2, −1, 0, 1, 2, representing homozygous deletion, single copy deletion, diploid normal copy, low-level copy number amplification, or high-level copy number amplification. Genes were mapped onto the human genome coordinates using UCSC cgData HUGO probeMap (https://tcga.xenahubs.net/download/TCGA.PANCAN.sampleMap/Gistic2_CopyNumber_Gistic2_all_thresholded.by_genes.gz).

Samples were subtyped based on PTEN copy number status, samples with CNV = 0 were assigned to PTEN normal (N = 6640), samples with CNV = −1 or −2 were assigned to PTEN copy number loss (N = 3422). PDHK1 gene expression was extracted from TCGA pan-cancer normalized RNaseq RFKM matrix and matched with samples with PTEN normal group (N = 5995) or PTEN copy number loss group (N = 2845).

Expression analysis of patient samples: Expression levels of PDHK1mRNA after normalization were compared between patient samples with single or double copy number loss of PTEN to patients with copy number neutral PTEN by boxplot analysis. The minimum, first quartile, median, third quartile and maximum were shown with horizontal lines from lower to upper with 1.5 interquartile range. Unfilled circles are outlier expression of PDHK1 in these two subgroups. Reported *p-value*s are for two-tailed unpaired t test with Welch's correction comparing the expression samples with PTEN copy number loss to the normal samples.

Survival analysis: Patient survival outcomes were downloaded from the Firehose web portal. We excluded from survival analysis patients over 75 years of age (N = 416) or patients who died less than 30 days from diagnosis (N = 184). Reported *p*-values are for a cox proportional hazards likelihood ratio test comparing a baseline model to a three-category model indicating a split of the patient cohort into three bins according to lower quartile (25 percentile and below), inter-quartile range (25-75 percentiles) and upper quartile (75 percentile and above) PDHK1 normalized expression values.

Gene expression array data analysis

Raw data was processed using R/Bioconductor package with Robust Multichip Average (RMA) normalization to identify differentially expressed genes between stable PTEN or GFP expressing H1650 cells. The normalized expression intensities were Log_2 transformed and multiple t test for null hypothesis was applied and adjusted with Benjamini-Hochberg's false discovery rate (FDR). The significantly differentially expressed genes were selected by applying fold change cut-off > 2, $^*p < 0.05$ and FDR adjusted *p*-value or *q*-value < 0.2.

Phospho-proteomics Data Analysis

Raw mass spectrometry data were analyzed using the MaxQuant software package (version 1.3.0.5). Data were matched to SwissProt reviewed entries for *Homo sapiens* in the UniProt protein database. MaxQuant was configured to generate and search against a reverse sequence database for false discovery rate calculations. Variable modifications were allowed for methionine oxidation, protein N terminus acetylation, and serine, threonine, and tyrosine phosphorylation. A fixed modification was indicated for cysteine carbamidomethylation. Full trypsin specificity was required. The first search was performed with a mass accuracy of ± 20 parts per million and the main search was performed with a mass accuracy of ± 6 parts per million. A maximum of 5 modifications were allowed per peptide. A maximum of 2 missed cleavages were allowed. The maximum charge allowed was 7+. Individual peptide mass tolerances were allowed. For MS/MS matching, a mass tolerance of 0.5 Da was allowed and the top 6 peaks per 100 Da were analyzed. MS/MS matching was allowed for higher charge states, water and ammonia loss events. The data were filtered to obtain a peptide, protein, and site-level false discovery rate of 0.01. The minimum peptide length was 7 amino acids. Results were matched between runs with a time window of 2 minutes for technical duplicates. The label-free PTEN phosphoproteomics data was analyzed using an in-house computational pipeline built for the analysis of post-translationally modified peptides with mixed effect models, implemented in the MSstats (v2.3.4) Bioconductor package(Choi et al., 2014). First, protein identifiers were converted into modification site identifiers, contaminant and false positive MaxQuant search results were removed and all samples were normalized per cell line by median-centering the log2-transformed MS1-intensity distributions. Next, the MSstats group Comparison function was run with the following options: no interaction terms for missing values, no interference, unequal intensity feature variance, restricted technical and biological scope of replication. Statistically significant changing sites between PTEN variants and the GFP control were selected by applying a Log_2 fold-change < - 0.5 and *q*-value < 0.05 threshold.

DATA AND CODE AVAILABILITY

Microarray data from this study have been deposited in GEO database (GEO: GSE121217). Phospho-proteomics data from this study have been deposited in PRIDE database (PRIDE: PXD014707).

Cell Reports, Volume *28*

Supplemental Information

Synthetic Essentiality of Metabolic Regulator PDHK1 in PTEN-Deficient Cells and Cancers

Nilanjana Chatterjee, Evangelos Pazarentzos, Manasi K. Mayekar, Philippe Gui, David V. Allegakoen, Gorjan Hrustanovic, Victor Olivas, Luping Lin, Erik Verschueren, Jeffrey R. Johnson, Matan Hofree, Jenny J. Yan, Billy W. Newton, John V. Dollen, Charles H. Earnshaw, Jennifer Flanagan, Elton Chan, Saurabh Asthana, Trey Ideker, Wei Wu, Junji Suzuki, Benjamin A. Barad, Yuriy Kirichok, James S. Fraser, William A. Weiss, Nevan J. Krogan, Asmin Tulpule, Amit J. Sabnis, and Trever G. Bivona

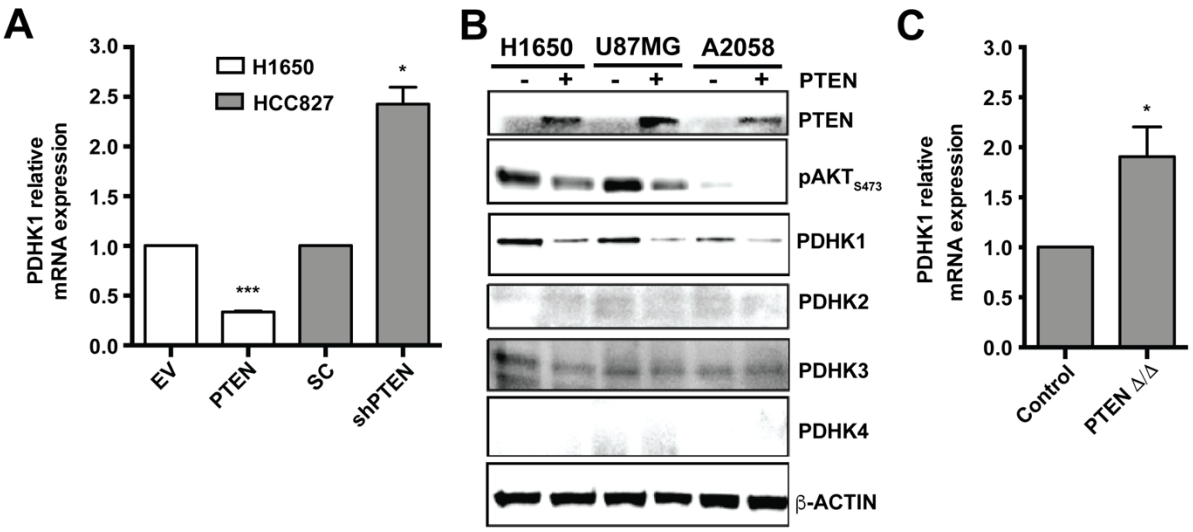

Figure S1

Figure S1. PTEN loss upregulates energy metabolism gene PDHK1 (related to Figure 1)
(A) Quantitative real-time RT-PCR analysis of PDHK1 mRNA expression in PTEN-deficient H1650 cancer cell line stably expressing empty vector (EV) or PTEN or in PTEN-proficient HCC827 cancer cell line with stable PTEN knockdown. shPTEN, shRNA to PTEN and SC, scrambled control shRNA. Data are shown as mean ± SEM (n = 3 replicates). ***$p < 0.001$ compared to 'empty vector expressing PTEN-deficient cells' or *$p < 0.05$ compared to 'scrambled control shRNA expressing PTEN-proficient cells' by two-tailed unpaired t test with Welch's correction. (B) Effects of adenovirus mediated transient PTEN re-expression in PTEN-deficient H1650, U87MG and A2058 cancer cell lines on phospho-AKT and PDHK1-4 expression by immunoblot analysis are shown. (C) Relative mRNA expression of PDHK1 by microarray analysis in lung epithelial cells with conditional PTEN deletion *in vivo* (GSE47520). Data are shown as mean ± SEM (n = 3 replicates). *$p < 0.05$ compared to 'PTEN expressing normal lung epithelial control cells' by two-tailed unpaired t test. PDHK1 probes: 1435836_at, 1423748_at, 1434974_at and 1423747_at.

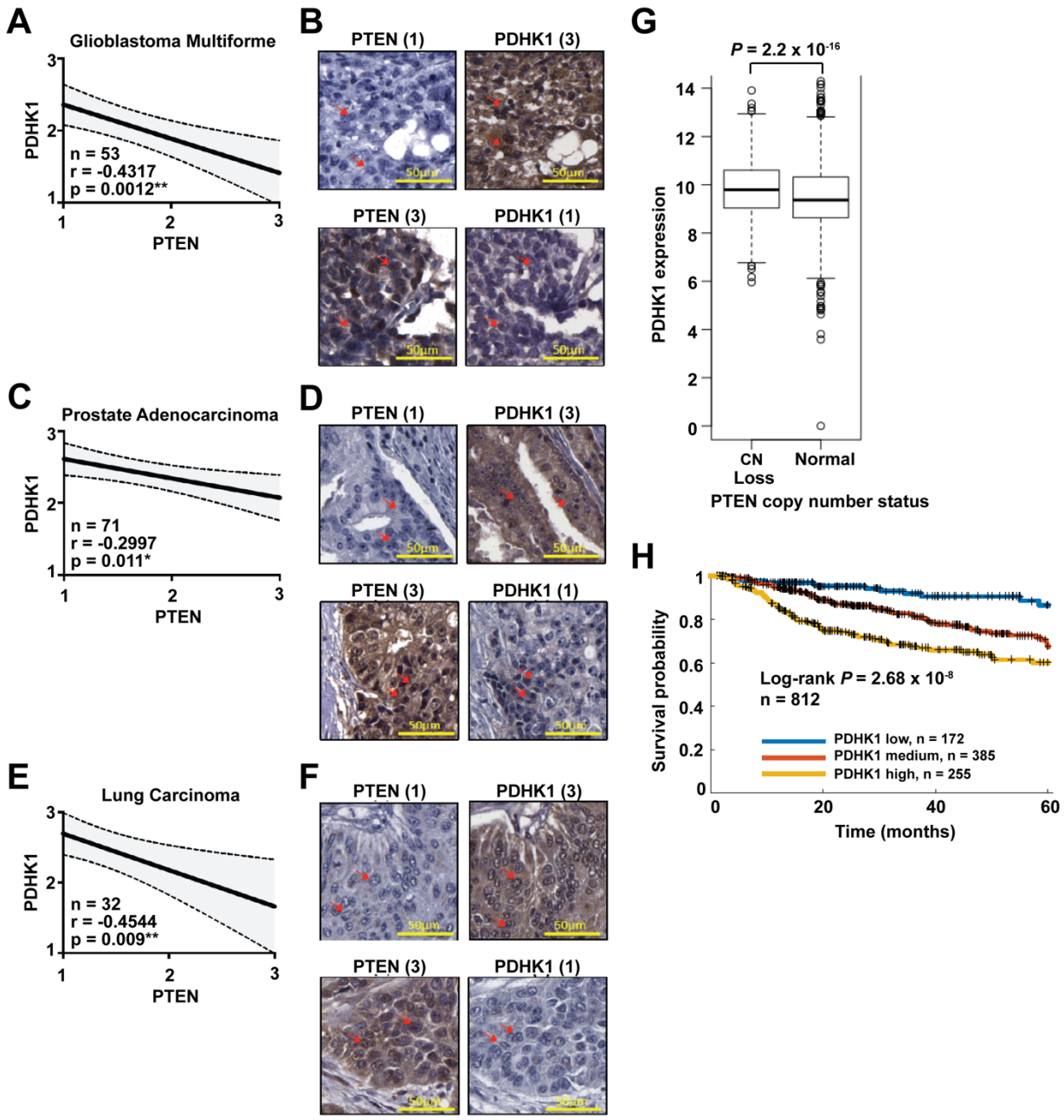

Figure S2

Figure S2. PTEN-deficient human tumors harbor increased PDHK1: a biomarker of worse patient survival (related to Figure 1)

(A, C, and E) Pearson correlation analysis to assess the relationship between PTEN and PDHK1 expression in the indicated patient tumor types as assessed by immunohistochemistry staining (STAR Methods). n, number of tumors analyzed, r, Pearson correlation coefficient where a negative value indicates inverse correlation and *p*-value, the significance of the correlation. $^{**}p < 0.01$, $^{*}p < 0.05$, as determined by two-tailed paired t-test analysis. (B, D, F) Representative IHC staining for PTEN and PDHK1 performed on tissue microarrays generated in the indicated tumor

types are shown. PTEN or PDHK1 expression scored on a scale of 1 to 3, with 1 indicating 'low', 2 'intermediate', and 3 'high' expression of each protein. Scale bar, 50 μm and arrows indicate representative tumor cells scored for PTEN and PDHK1 expression. (G) Box plots indicating median (black bar), interquartile range (black box) and total range (whiskers) of normalized PDHK1 mRNA expression levels in TCGA multi tissue pan-cancer (12 cancer types) with PTEN normal (n = 5995) or single or double copy number (CN) loss (n = 2845) are shown. Unfilled circles are outliers of PDHK1 mRNA expression in these two subgroups. $P = 2.2 \times 10^{-16}$ 'compared to PTEN normal samples' by two-tailed unpaired t test with Welch's correction. (H) 5-year survival Kaplan-Meier analysis of PTEN CN loss patients with either high, intermediate or low level of normalized PDHK1 mRNA expression in the cancer datasets in G.

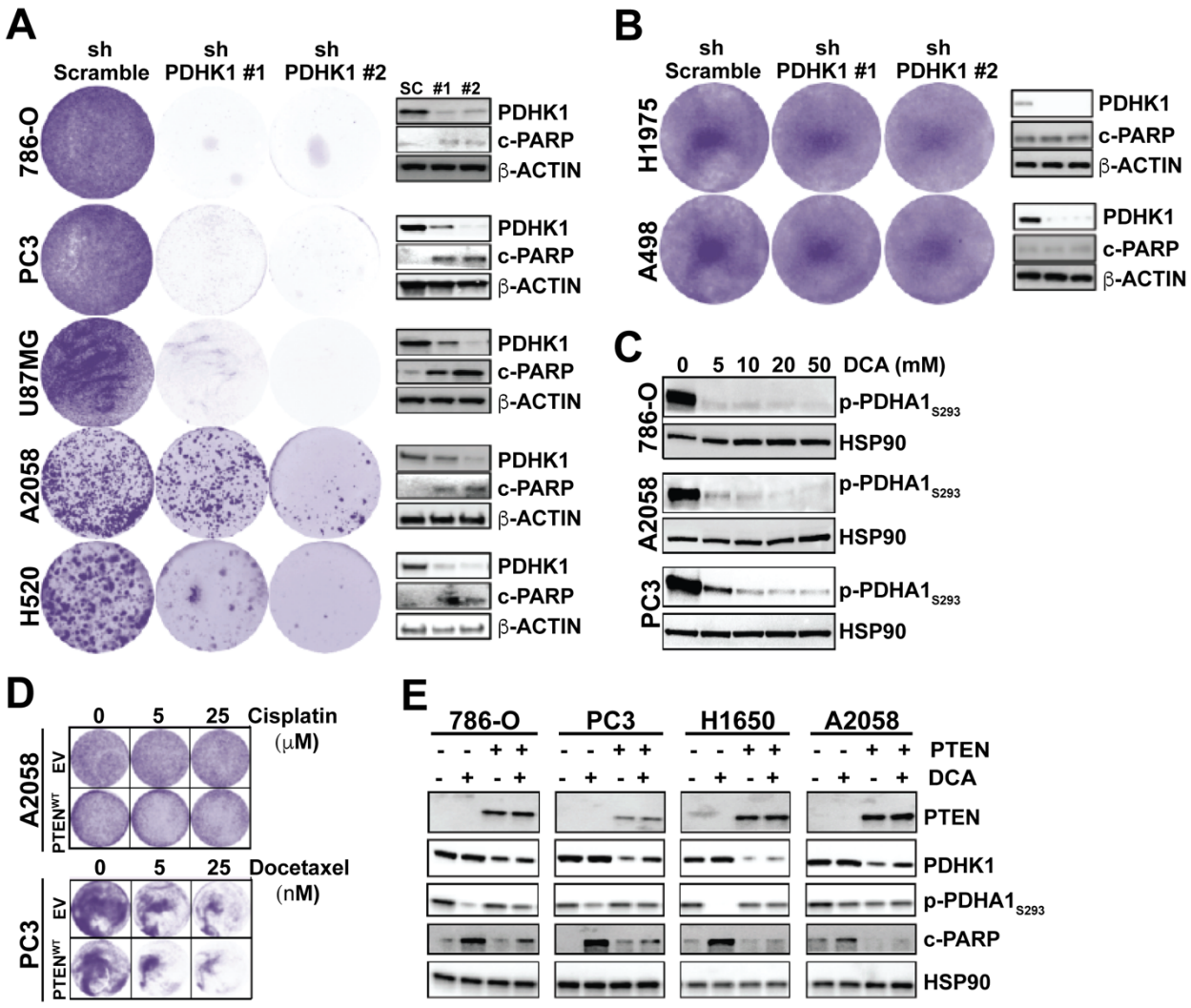

Figure S3

Figure S3. PTEN loss or inactivation renders cells dependent on PDHK1 for survival (related to Figure 2)

(A) Effects of stable PDHK1 knockdown in various PTEN-deficient (A) or -proficient cancer cell lines (B) on cell growth by crystal violet staining assay (left) and apoptosis induction as measured by cleaved PARP levels by immunoblot analysis (right) are shown. shPDHK1#1 and shPDHK1#2, shRNAs to PDHK1 and shScramble, scrambled control shRNA. (C) Western blots showing phospho-PDHA1 expression in PTEN-deficient cancer cell lines in response to PDHK1 inhibition by DCA (dose response: 0, 5, 10, 20, 50 mM) or vehicle (water) treatment. (D) Effects of chemotherapeutic agents used at indicated concentrations on cell growth of PTEN-deficient cancer cell lines stably expressing empty vector (EV) or PTEN by crystal violet staining assay are shown. (E) Effects of pharmacologic inhibition of PDHK1 with 25 mM DCA in PTEN-deficient cancer cell lines with or without stable PTEN re-expression on pyruvate dehydrogenase complex (PDC) activation and apoptosis induction as measured by phospho-PDHA1 and cleaved PARP levels, respectively, by western blot are shown.

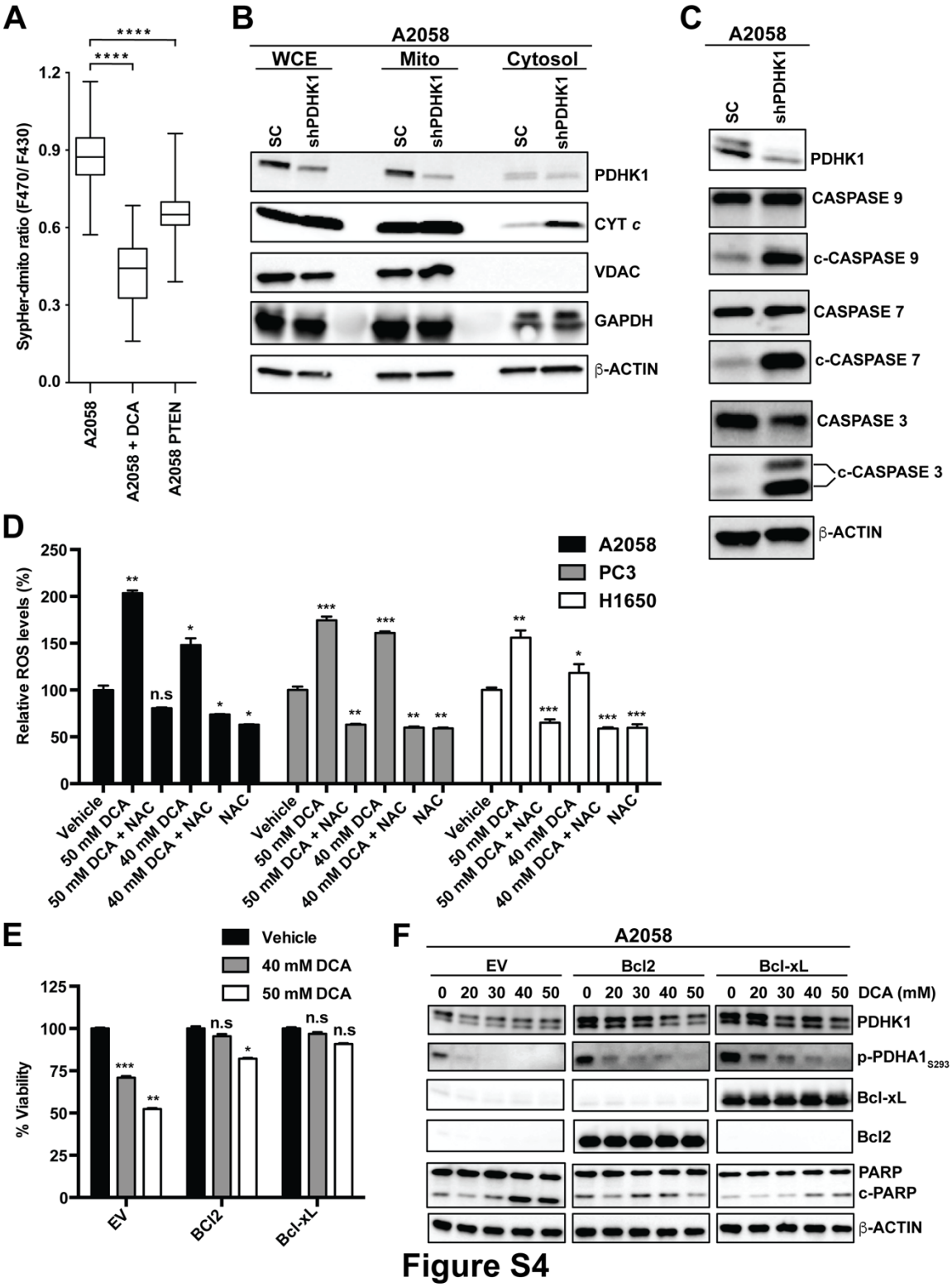
A
B
C
D
E
F
SypHer-dmito ratio (F470/ F430)
A2058
A2058 + DCA
A2058 PTEN
WCE
Mito
Cytosol
SC
shPDHK1
PDHK1
CYT c
VDAC
GAPDH
β-ACTIN
CASPASE 9
c-CASPASE 9
CASPASE 7
c-CASPASE 7
CASPASE 3
c-CASPASE 3
Relative ROS levels (%)
PC3
H1650
Vehicle
50 mM DCA
50 mM DCA + NAC
40 mM DCA
40 mM DCA + NAC
NAC
% Viability
EV
BCl2
Bcl-xL
n.s
DCA (mM)
p-PDHA1S293
Bcl-xL
Bcl2
PARP
c-PARP

Figure S4

Figure S4. PDHK1 suppression in PTEN-deficient cells induce apoptosis by multiple mechanisms (related to Figure 2)

(A) Box plots indicating median (black bar), interquartile range (black box) and total range (whiskers) of F470/F430 ratio of SypHer-dmito in PTEN-deficient A2058 cancer cells (n = 1503), in 50 mM DCA treated A2058 cancer cells (n = 1500) and in A2058 cancer cells stably expressing PTEN (n = 773) are shown. ****$p < 0.0001$ 'compared to PTEN-deficient A2058 cells' by multiple comparisons Kruskal-Wallis test. (B) Effects of stable PDHK1 knockdown in PTEN-deficient cancer cell line A2058 on cytochrome *c* subcellular localization by mitochondrial-cytoplasmic fractionation and immunoblotting are shown. Western blots were also probed with anti-VDAC and anti-GAPDH antibodies as mitochondrial and cytoplasmic markers, respectively. shPDHK1, shRNA to PDHK1 and SC, scrambled control shRNA. In addition to the cytoplasm where majority of GAPDH is located under basal condition, GAPDH is also found in other subcellular compartments such as, mitochondria, under different stress conditions (Tristan et al., 2011), as seen over here. (C) Effects of stable PDHK1 knockdown in PTEN-deficient cancer cell line A2058 on caspase activation as measured by cleaved caspase 9, cleaved caspase 7 and cleaved caspase 3 levels by immunoblotting are shown. Western blots were also probed with anti-actin β antibody as loading control. shPDHK1, shRNA to PDHK1 and SC, scrambled control shRNA. (D) Effects of pharmacologic inhibition of PDHK1 in PTEN-deficient cancer cell lines with DCA (dose response: 0, 40 and 50 mM) or vehicle (RPMI without phenol red) treatment for 24 hours on intracellular ROS levels were determined by DCF or 2',7'-dichlorofluorescein fluorescence. 1 mM NAC (N-Acetyl cysteine: a validated ROS scavenger) treatment was used as a negative control to lower ROS levels (Sun, 2010). Data are shown as mean ± SM (n = 4 replicates). *$p < 0.05$; **$p < 0.01$; ***$p < 0.001$; n.s, not significant compared to 'vehicle treated cells' by Dunnett's multiple comparisons one-way ANOVA test. (E) Effects of pharmacologic inhibition of PDHK1 and lentivirus-based stable empty vector (EV) or Bcl2 or Bcl-xL expression in PTEN-deficient cancer cell line A2058 with DCA (dose response: 0, 40 and 50 mM) or vehicle (DMEM) treatment for 24 hours on cell viability by CellTiter-Glo luminescent assay are shown. Data are shown as mean ± SM (n = 3 replicates). *$p < 0.05$; **$p < 0.01$; ***$p < 0.001$; n.s, not significant compared to 'vehicle treated cells' by Dunnett's multiple comparisons one-way ANOVA test. (F) Effects of pharmacologic inhibition of PDHK1 and lentivirus-based stable empty vector (EV) or Bcl2 or Bcl-xL expression in PTEN-deficient cancer cell line A2058 with DCA (dose response: 0, 20, 30, 40 and 50 mM) or vehicle (DMEM) treatment for 48 hours on pyruvate dehydrogenase complex (PDC) activation and apoptosis induction as measured by phospho-PDHA1 and cleaved PARP levels, respectively, by western blot are shown.

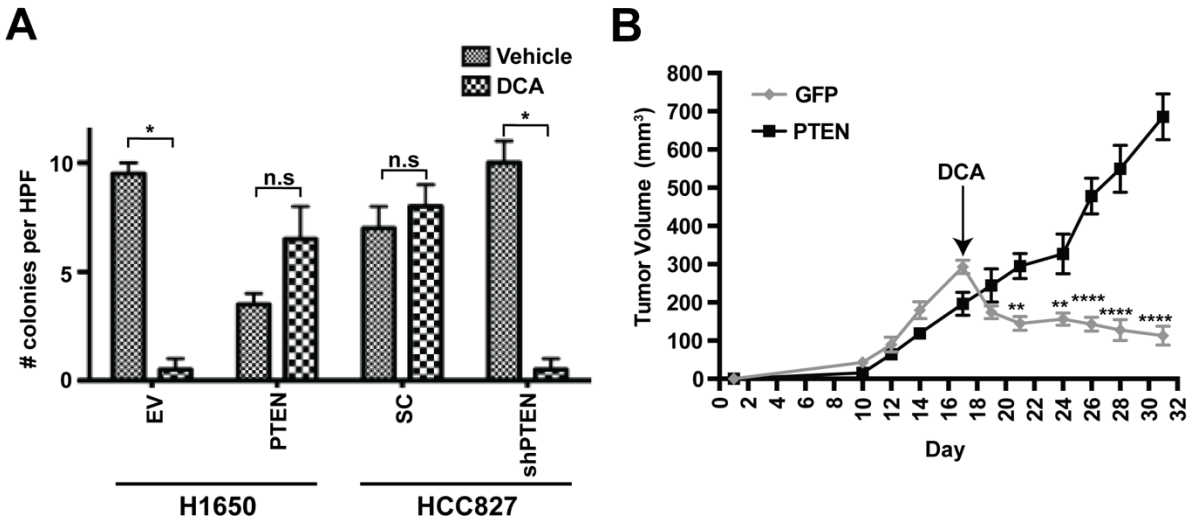

Figure S5

Figure S5. PTEN deficiency combined with PDHK1 inhibition suppresses colony formation *in vitro* and tumor xenograft growth *in vivo* (related to Figure 2)

(A) Effects of pharmacologic inhibition of PDHK1 with DCA or vehicle (water) treatment in PTEN-deficient H1650 cancer cell line stably expressing PTEN or PTEN-proficient HCC827 cancer cell line with stable PTEN knockdown on colony formation by *in vitro* colony formation assay are shown as measured by the number of colonies counted per high-power field (HPF: 400 x magnification). Data are shown as mean ± SEM (n = 3 replicates). *$p < 0.05$; n.s, not significant compared to 'vehicle treated cells' by Student's t test. (B) Effects of pharmacologic inhibition of PDHK1 with DCA in A2058-PTEN or GFP melanoma xenografts on tumor growth *in vivo*. Data are shown as mean ± SEM, n = 6 tumors/ group. **$p < 0.01$, ****$p < 0.0001$ compared to 'PTEN-deficient GFP expressing A2058 cells' by two-way ANOVA Sidak's multiple comparisons test.

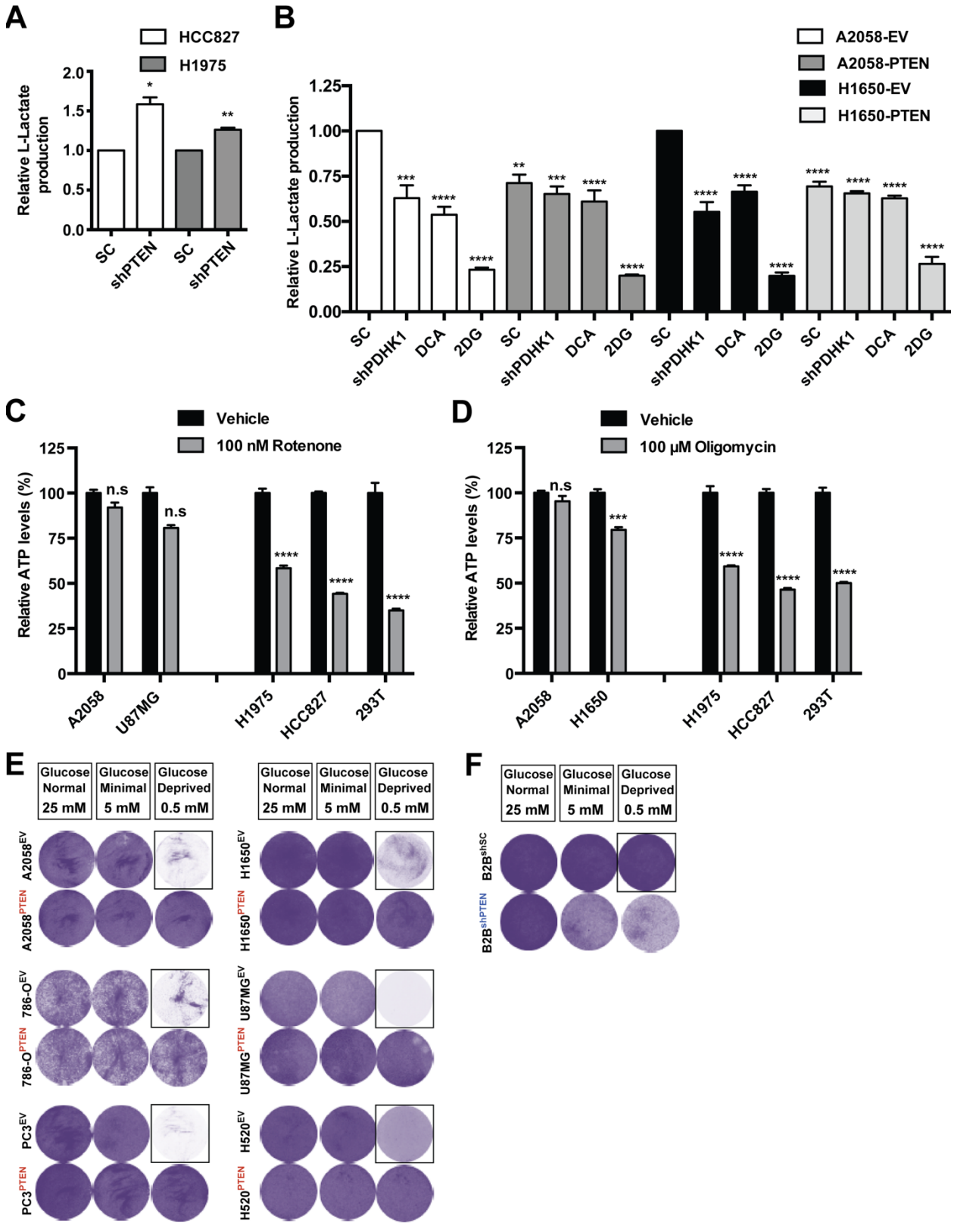
A
HCC827
H1975
Relative L-Lactate production
SC
shPTEN
B
A2058-EV
A2058-PTEN
H1650-EV
H1650-PTEN
Relative L-Lactate production
SC
shPDHK1
DCA
2DG
C
Vehicle
100 nM Rotenone
Relative ATP levels (%)
n.s
A2058
U87MG
H1975
HCC827
293T
D
Vehicle
100 µM Oligomycin
Relative ATP levels (%)
A2058
H1650
H1975
HCC827
293T
E
Glucose Normal 25 mM
Glucose Minimal 5 mM
Glucose Deprived 0.5 mM
A2058EV
A2058PTEN
H1650EV
H1650PTEN
786-OEV
786-OPTEN
U87MGEV
U87MGPTEN
PC3EV
PC3PTEN
H520EV
H520PTEN
F
Glucose Normal 25 mM
Glucose Minimal 5 mM
Glucose Deprived 0.5 mM
B2BshSC
B2BshPTEN

Figure S6

Figure S6. PTEN loss promotes glucose dependence and aerobic glycolysis via PDHK1 (related to Figure 2)

(A) Effects of stable PTEN knockdown in PTEN-proficient cancer cell lines on L-lactate production by measuring extracellular lactate in an *in vitro* coupled fluorescent assay (STAR Methods) are shown. shPTEN, shRNA to PTEN and SC, scrambled control shRNA. Data are shown as mean ± SEM (n = 3 replicates). *$p < 0.05$; **$p < 0.01$ compared to 'scrambled control shRNA expressing PTEN-deficient cells' by two-tailed unpaired t test with Welch's correction. (B) Effects of stable PDHK1 knockdown or PDHK1 inhibition with 10 mM DCA in PTEN-deficient cancer cells stably expressing empty vector (EV) or PTEN on L-lactate production by measuring extracellular lactate in an *in vitro* coupled fluorescent assay are shown. 2DG (2-deoxyglucose) was used as a +ve control to suppress lactate production independently. shPDHK1, shRNA to PDHK1 and SC, scrambled control shRNA. Data are shown as mean ± SEM (n = 3 replicates). ****$p < 0.0001$; ***$p < 0.001$; **$p < 0.01$ compared to 'scrambled control shRNA expressing PTEN-deficient cells' by Dunnett's multiple comparisons one-way ANOVA test. (C-D) Effects of pharmacologic inhibition of oxidative phosphorylation in PTEN-deficient (left) or -proficient (right) cancer and normal cell lines treated with vehicle (DMSO) or 100 nM rotenone (electron transport chain complex I inhibitor) for 2 hours (C) or 100 μM oligomycin (electron transport chain complex V inhibitor) for 1 hour (D) after 24 hours of cell seeding on ATP production by CellTiter-Glo luminescent assay are shown. Data are shown as mean ± SM (n = 3 replicates). ****$p < 0.0001$; ***$p < 0.001$; n.s, not significant compared to 'vehicle treated cells' by Sidak's multiple comparisons two-way ANOVA test. (E-F) Effects of glucose deprivation in culture media of PTEN-deficient cancer cell lines stably expressing empty vector (EV) or PTEN (E) or PTEN-proficient normal cells with stable PTEN knockdown (F) on cell growth by crystal violet staining assay are shown. shPTEN, shRNA to PTEN and SC, scrambled control shRNA. Standard (25 mM) glucose replete media was used as control.

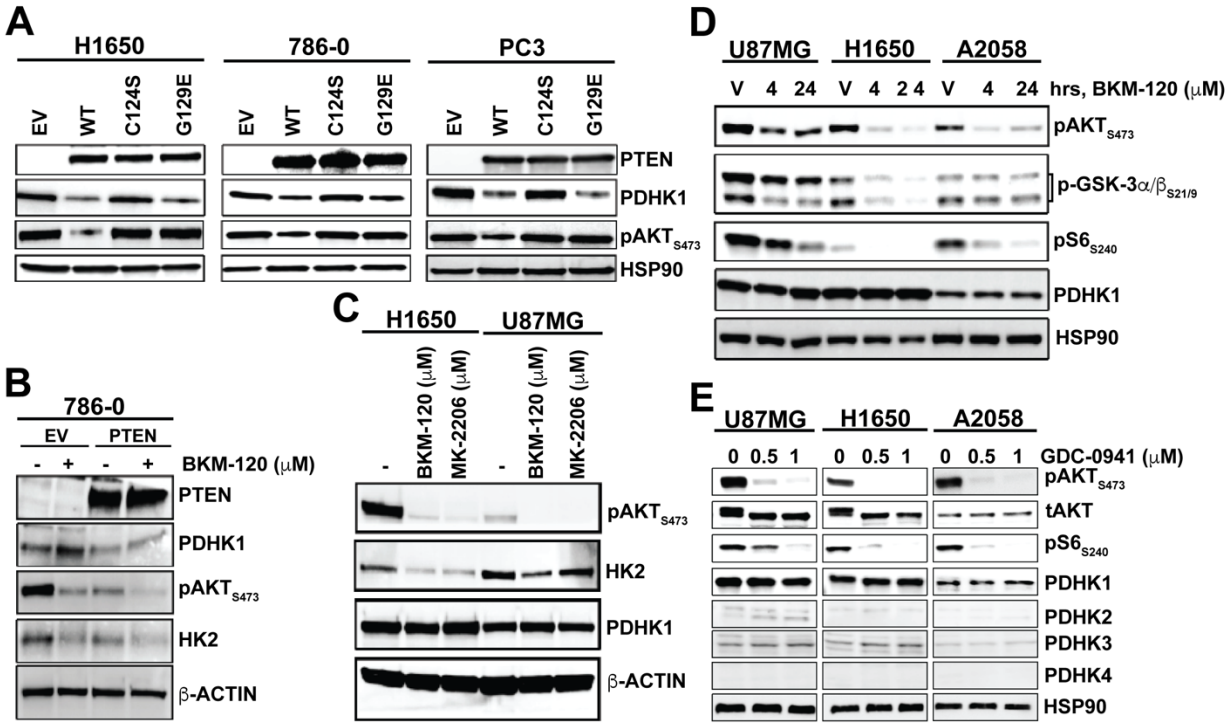

Figure S7

Figure S7. PTEN regulates PDHK1 via its protein, and not lipid, phosphatase activity in a PI3K-AKT independent manner (related to Figure 3)

(A) Western blots showing PTEN, PDHK1 and phospho-AKT expression in PTEN-deficient cancer cell lines stably expressing $PTEN^{WT}$ or $PTEN^{G129E}$ or $PTEN^{C124S}$ or empty vector (EV). (B) Effects of PI3K inhibition with BKM-120 or vehicle (DMSO) treatment in PTEN-deficient 786-O cancer cells stably expressing empty vector (EV) or PTEN for 24 hours on PDHK1, phospho-AKT and HK2 expression by immunoblotting analysis are shown. (C) Effects of PI3K or AKT inhibition in PTEN-deficient cancer cell lines treated for 24 hours with BKM-120 or MK-2206 on phospho-AKT, HK2 and PDHK1 expression by immunoblotting analysis are shown. (D) Effects of PI3K inhibition in PTEN-deficient cancer cell lines treated for 4-24 hours with BKM120 on phospho-AKT, phospho-GSK3, phospho-S6 and PDHK1 expression by immunoblotting analysis are shown. V: vehicle (DMSO) treatment. (E) Effects of PI3K inhibition in PTEN-deficient cancer cell lines treated with GDC-0941 (0, 0.5, 1 μM) for 24 hours on phospho-AKT, total AKT, phospho-S6 and PDHK1-4 expression by immunoblotting analysis are shown. PI3K or AKT inhibitors were used at 1 μM final concentration for the indicated times in B-D.

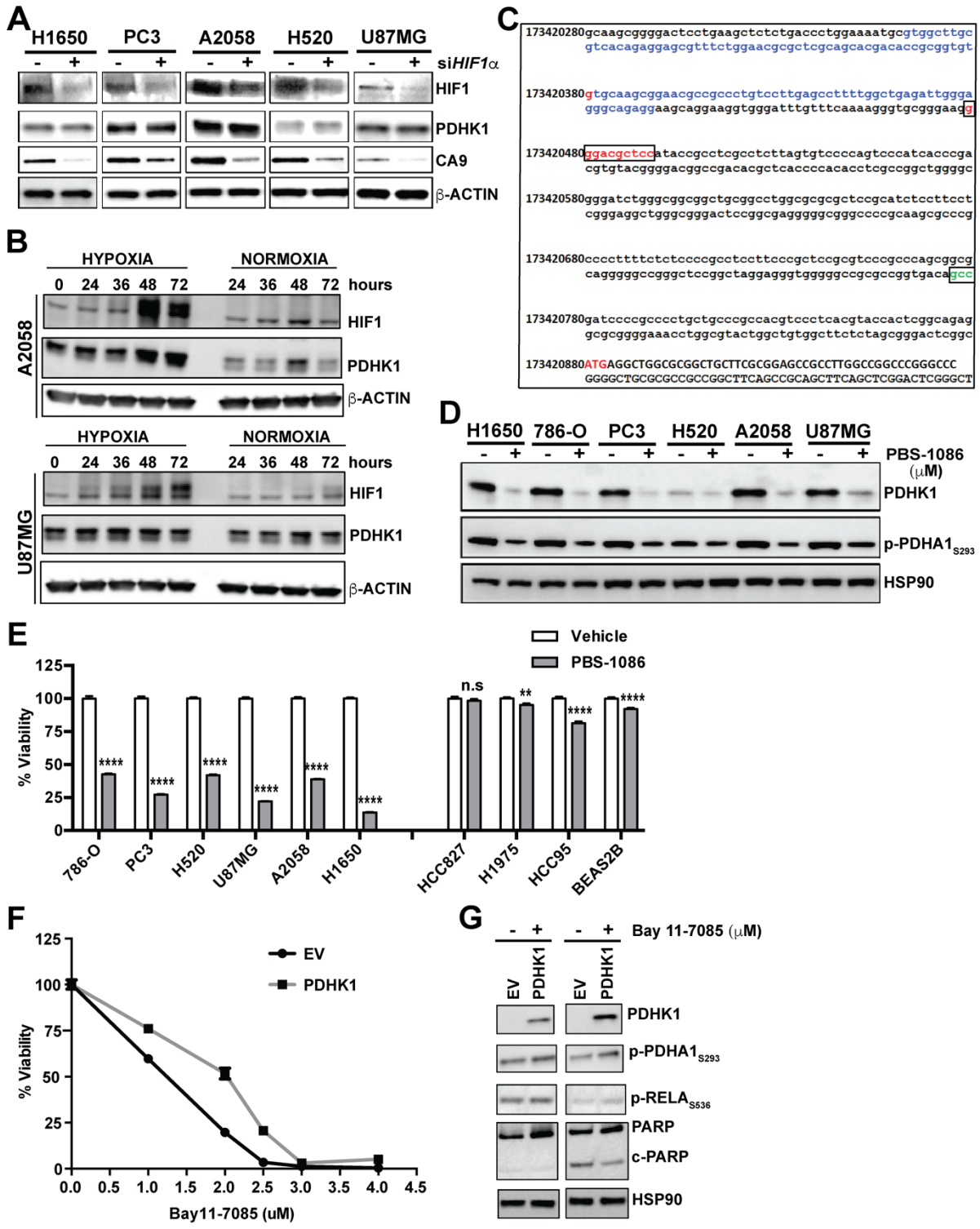

Figure S8

Figure S8. PTEN regulates PDHK1 via NF-κB and PTEN deficiency combined with NF-κB inhibition decreases cell viability (Related to Figure 4)

(A) Effects of transient HIF1α knockdown in PTEN-deficient cancer cell lines on HIF1α, PDHK1 and CA9 expression by immunoblotting are shown. siHIF1α, HIF1α specific small interfering RNA and sc (-), scrambled control siRNA. (B) Differential expression patterns of HIF1α and PDHK1 in PTEN-deficient cancer cell lines after 0, 24, 36, 48 and 72 hours of incubation under hypoxia versus normoxia by immunoblotting are shown. (C) PDHK1 promoter sequence analysis. The canonical NF-κB binding site (GGGACGCTCC, highlighted in red and boxed) is located between nucleotide positions 173420479 and 173420488 in chromosome 2, ~300 bp upstream of the transcription start site (TSS, highlighted in green and boxed). 118 bp region (highlighted in blue) spanning nucleotide position 173420380 (highlighted in red) ~40 bp upstream of the NF-κB binding site in the PDHK1 promoter was probed for NF-κB recruitment by ChIP assay. ATG: start of PDHK1 gene, highlighted in red. (D) Western blots showing PDHK1 and phospho-PDHA1 expression in PTEN-deficient cancer cell lines in response to 10 μM PBS-1086 (NF-κB or REL inhibitor) or vehicle (DMSO) treatment. (E) Effects of pharmacologic inhibition of NF-κB in PTEN- deficient (left) or - proficient (right) cancer cell lines treated with 10 μM PBS-1086 (NF-κB or REL inhibitor) or vehicle (DMSO) for 72 hours on cell viability by CellTiter-Glo luminescent assay are shown. Data are shown as mean ± SM (n = 16 replicates). ****$p < 0.0001$; **$p < 0.001$; n.s, not significant compared to 'vehicle treated cells' by Sidak's multiple comparisons two-way ANOVA test. (F) Effects of pharmacologic inhibition of NF-κB and lentivirus-based stable EV (empty vector) or PDHK1 expression in PTEN-deficient cancer cell line A2058 with Bay 11-7085 (dose response: 0, 1, 2, 2.5, 3 and 4 μM) or vehicle (DMSO) treatment for 48 hours on cell viability by CellTiter-Glo luminescent assay are shown. Data are shown as mean ± SM (n = 4 replicates). (G) Effects of pharmacologic inhibition of NF-κB and lentivirus-based stable PDHK1 or EV (empty vector) expression in PTEN-deficient cancer cell line A2058 with Bay 11-7085 (dose response: 0, 1, 2, 2.5, 3 and 4 μM) or vehicle (DMSO) treatment for 48 hours on pyruvate dehydrogenase complex (PDC) activation and apoptosis induction as measured by phospho-PDHA1 and cleaved PARP levels, respectively, by western blot analysis are shown.

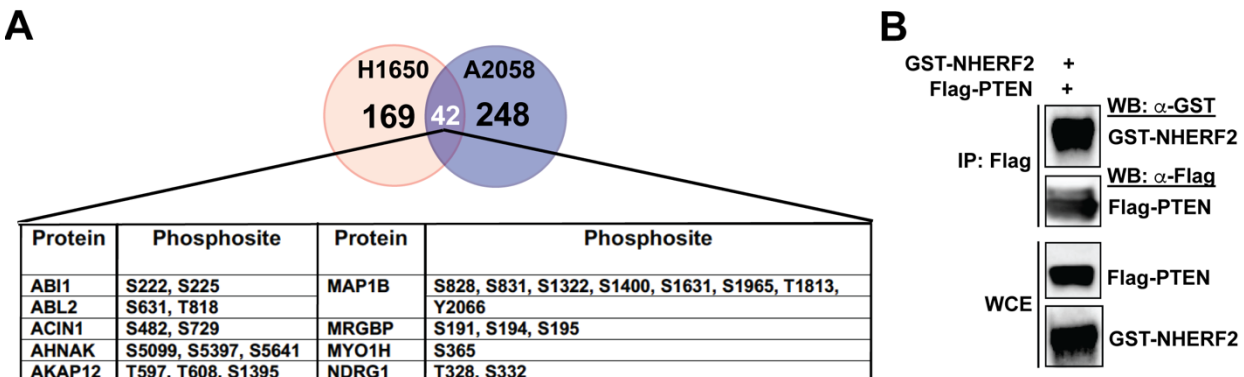

Protein	Phosphosite	Protein	Phosphosite
ABI1	S222, S225	MAP1B	S828, S831, S1322, S1400, S1631, S1965, T1813,
ABL2	S631, T818		Y2066
ACIN1	S482, S729	MRGBP	S191, S194, S195
AHNAK	S5099, S5397, S5641	MYO1H	S365
AKAP12	T597, T608, S1395	NDRG1	T328, S332
AKAP2	S630, S748	NKAP	S9, S149
APC	T1438, S2283	NUMA1	S1225, T2000
ATP2B1	S1253, T1256	PALLD	S1101, S1104
ATXN2	T741, S843, S849	PML	S403, S505
BAG3	S274, S275, S279	RBMX2	S185, S188
CAP2	S30, S301, S312	RSF1	S473, S622, S629
CLASP1	S572, S686	SAFB	T374, S384, S601, S604
CLASP2	S455, S459, S1012	SPEN	S727, S1287
DDX42	Y183, S754	SRRM1	T416, S695, S769, S773, S775, S781
FARP1	S424, S433	SRRM2	T328, T1856, T2104, Y967, S398, S562, S564, S566,
HNRPD	S80, S83		S884, S972, S972, S973, S974, S1014, S1102,
INCENP	S481, T892		S1112, S1598, S1600, S1601, S1857, S2100, S2123,
KLC2	S501, S508	STIP1	S16, S481
LMNA	S392, S403, S404,	SYNPO	S285, S685, S698
	S406, S407, S414	TCOF1	T914, S1228
LMNB1	T20, S85, S387, S391,	TOR1AIP1	S157, S163, S242
	S393	TRA2B	T203, T260, S264
LUZP1	S394, S905	UBR4	S362, S625, S2722, T360, T2724
MACF1	S4496		

Figure S9

Figure S9, Identification of phospho-proteins, including NKAP, that are specifically regulated by the PTEN protein phosphatase activity in cells (Related to Figure 5)

(A) Phospho-proteins (n=42, listed alphabetically), including NKAP (highlighted in red box), regulated specifically by the PTEN protein-phosphatase in both H1650 and A2058 PTEN-deficient cancer cell lines stably expressing either $PTEN^{WT}$ or $PTEN^{G129E}$ or $PTEN^{Y138L}$ or GFP identified by an unbiased global phospho-proteomic profiling analysis (STAR Methods) are shown. Venn diagram representation of the phospho-proteins regulated specifically by the PTEN protein phosphatase in either H1650 (n = 169) or A2058 (n = 248) or both (n = 42) cell lines. (B) Co-immunoprecipitation of NHERF2 with PTEN upon over-expression of both GST-NHERF2 and FLAG-PTEN in 293T cells followed by IP-FLAG is shown.

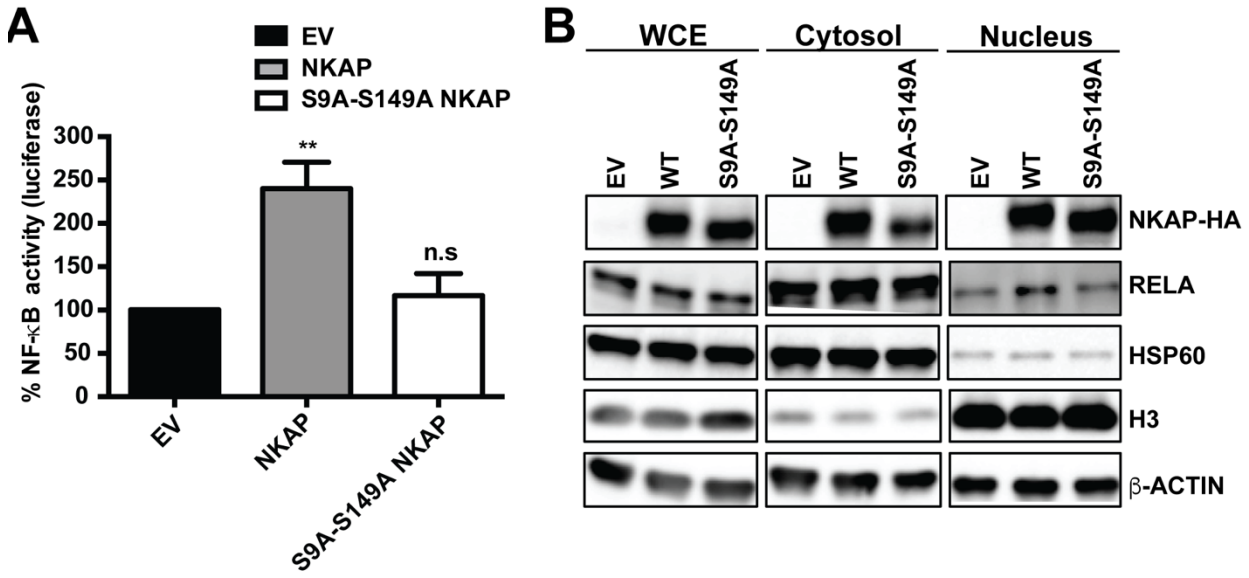

Figure S10

Figure S10. NKAP^{WT}, but not de-phosphorylation deficient-mutant NKAP$^{S9A-S149A}$, enhances NF-κB transcriptional activity and NF-κB nuclear localization (Related to Figure 6)

(A) Effects of empty vector (EV) or HA-NKAP^{WT} or HA-NKAP$^{S9A-S149A}$ expression in PTEN-deficient A2058 cancer cell line on NF-κB transcriptional activity by luciferase reporter assays (STAR Methods) are shown. Data are shown as mean ± SEM (n = 3 replicates). $^{**}p < 0.01$; n.s, not significant compared to 'empty vector control expressing PTEN-deficient A2058 cells' by Dunnett's multiple comparisons one-way ANOVA test. (B) Effects of HA-NKAP^{WT} or HA-NKAP$^{S9A-S149A}$ or empty vector (EV) expression in PTEN-deficient A2058 cancer cell line on NF-κB (RELA) subcellular localization by nuclear-cytoplasmic fractionation and immunoblotting are shown. Western blots were also probed with H3 and HSP60 antibodies as nuclear and cytoplasmic markers, respectively.

Cell Line	Type	Origin	PTEN gene status	Expression
H1650	Lung Adenocarcinoma	Lung	HOMDEL (exon 8, 9)	-
H1975	Lung Adenocarcinoma	Lung	No alteration	+
HCC827	Lung Adenocarcinoma	Lung	No alteration	+
HCC95	Lung Squamous Carcinoma	Lung	No alteration	+
PC3	Prostate Adenocarcinoma	Prostate	R55fs*1	-
786-O	Renal Clear Cell Carcinoma	Kidney	Q149* (STOP)	-
H520	Lung Squamous Carcinoma	Lung	No alteration*	-
A2058	Skin Cutaneous Melanoma	Skin	L112Q	-
U87MG	Glioblastoma Multiforme	Brain	L70_splice	-
293T	Human Embryonic Kidney	Kidney	No alteration	+
BEAS2B	Bronchial Epithelial Normal cells	Bronchus	No alteration	+

Table S1. Genetic and expression status of PTEN in cell lines (related to Figure 1)
The genetic status of PTEN in cancer and normal cell lines was determined from the Cancer Cell Line Encyclopedia (CCLE). (-) indicates PTEN-deficient and (+) indicates PTEN-expressing cells. *PTEN gene silencing occurs by promoter methylation (Millan-Ucles et al., 2016; Soria et al., 2002) in H520 cell line.

Gene Symbol	**<u>Upregulated</u>** Fold change (GFP vs PTEN)	***p*-value**	**q-value** (FDR adj *p*-value)
NPR3	2.97	0.002	0.15
STC1	2.81	0.000	0.13
CP	2.65	0.005	0.17
PFKFB4	2.54	0.001	0.13
MT1X	2.40	0.001	0.13
ARTN	2.38	0.009	0.19
PDHK1	2.33	0.006	0.17
ZNF711	2.22	0.006	0.17
SLC2A14	2.15	0.011	0.20
DDIT4	2.03	0.003	0.16
DSG3	2.01	0.006	0.17
Gene Symbol	**<u>Downregulated</u>** Fold change (GFP vs PTEN)	***p*-value**	**q-value** (FDR adj *p*-value)
NECTIN3-AS1	0.50	0.001	0.14
AGO4	0.50	0.011	0.20
PCGF5	0.50	0.002	0.15
APPBP2	0.50	0.009	0.19
GIMAP2	0.49	0.000	0.13
DPYSL2	0.49	0.009	0.19
ANXA8L1	0.48	0.003	0.16
ANXA8	0.48	0.003	0.16
TENM2	0.48	0.005	0.17
HHAT	0.48	0.001	0.14
GATA6	0.48	0.007	0.18
GJA5	0.47	0.002	0.15
SAP30L	0.47	0.005	0.17
BNC1	0.46	0.000	0.12
MGARP	0.46	0.001	0.14
PCM1	0.45	0.009	0.19
AMPH	0.44	0.002	0.15
ERFE	0.44	0.006	0.18
TMEM237	0.44	0.003	0.15
ENO1P4	0.44	0.003	0.15
GLB1L3	0.44	0.001	0.14
CTGF	0.43	0.000	0.13
RARRES1	0.43	0.002	0.15
ANOS1	0.43	0.007	0.18
MAMDC2	0.43	0.006	0.17
RPS6KA2	0.42	0.002	0.15
BMP2	0.42	0.008	0.19
CDYL2	0.40	0.000	0.12
IGDCC4	0.40	0.001	0.13
BEND7	0.39	0.005	0.17
CFAP58	0.39	0.006	0.18
GNG4	0.37	0.004	0.16
SERPINE2	0.34	0.000	0.13
RFTN1	0.33	0.004	0.16
HTRA1	0.33	0.010	0.20
NECTIN3	0.33	0.007	0.18
IGFBP7	0.28	0.000	0.13

COL13A1	0.25	0.002	0.15
EVI2B	0.22	0.002	0.15
CES1P1	0.19	0.010	0.19
CES1	0.19	0.010	0.19

Table S2. List of genes significantly differentially expressed in response to PTEN status (related to Figure 1)

Genes upregulated (including PDHK1, highlighted in red) or downregulated in PTEN-deficient H1650 cells are listed. 52 genes were significantly differentially expressed between stable PTEN and GFP expressing H1650 cells by microarray analysis (fold change > 2, multiple t-tests $*p < 0.05$, FDR adjusted p-value or $q < 0.2$, n = 3 replicates).

Gene Symbol	Gene Symbol	Gene Symbol	Gene Symbol
AHR	E2	HSF2	PAX2
AHRARNT	E2F	IK1	PAX5
AML1	E47	IK2	PAX6
AP1	E4BP4	IK3	R
AP2	EGR1	LMO2COM	RREB1
AP4	EGR2	LYF1	SEF1
ARP1	EGR3	MYOD	SP1
ATF	ELK1	MYOGNF1	SREBP1
CAAT	ER	MZF1	SRY
CAP	GATA1	NF1	STAF
CDPCR3	GATA2	**NF-κB**	STAT
CEBP	GATA3	NFY	T3R
CEBPB	GC	NGFIC	TATA
CETS1P54	GFI1	NMYC	TAXCREB
CMYB	GR	NRF2	USF
COMP1	GRE	NRSF	VBP
CP2	HEN1	1-Oct	VMYB
CREB	HLF	OLF1	YY1
CREBP1	HNF4	P300	ZID
DELTAEF1	HSF1	P53	

Table S3. List of transcription factors with consensus binding sites in the PDHK1 promoter, including NF-κB (related to Figure 4) Human PDHK1 promoter sequence (-499 bp from TSS) was retrieved from Eukaryotic Promoter Database (https://epd.vital-it.ch/index.php) and analyzed for transcription factor binding sites using TFBIND tool (http://tfbind.hgc.jp/) based on position weight matrix algorithm (TRANSFAC R.3.4) (Tsunoda and Takagi, 1999). Eighty-two different transcription factors, including NF-κB (highlighted in red), with high TF binding score (> 0.8) were identified and are listed.